# Black hole mass measurement using molecular gas kinematics: what ALMA can do

## Ilsang Yoon[1,2]★

[1]*National Radio Astronomy Observatory, 520 Edgemont Road, Charlottesville, VA 22903, USA*
[2]*Leiden Observatory, Leiden University, PO Box 9513, NL-2300 RA Leiden, The Netherlands*

## ABSTRACT

We study the limits of the spatial and velocity resolution of radio interferometry to infer the mass of supermassive black holes (SMBHs) in galactic centres using the kinematics of circumnuclear molecular gas, by considering the shapes of the galaxy surface brightness profile, signal-to-noise ratios (S/Ns) of the position–velocity diagram (PVD) and systematic errors due to the spatial and velocity structure of the molecular gas. We argue that for fixed galaxy stellar mass and SMBH mass, the spatial and velocity scales that need to be resolved increase and decrease, respectively, with decreasing Sérsic index of the galaxy surface brightness profile. We validate our arguments using simulated PVDs for varying beam size and velocity channel width. Furthermore, we consider the systematic effects on the inference of the SMBH mass by simulating PVDs including the spatial and velocity structure of the molecular gas, which demonstrates that their impacts are not significant for a PVD with good S/N unless the spatial and velocity scale associated with the systematic effects are comparable to or larger than the angular resolution and velocity channel width of the PVD from pure circular motion. Also, we caution that a bias in a galaxy surface brightness profile owing to the poor resolution of a galaxy photometric image can largely bias the SMBH mass by an order of magnitude. This study shows the promise and the limits of ALMA observations for measuring SMBH mass using molecular gas kinematics and provides a useful technical justification for an ALMA proposal with the science goal of measuring SMBH mass.

**Key words:** black hole physics – methods: observational – ISM: kinematics and dynamics – galaxies: nuclei.

## 1 INTRODUCTION

Supermassive black holes (SMBHs) in galactic centres influence the formation and evolution of the host galaxies (Richstone et al. 1998; Kormendy & Ho 2013) as suggested by well-known empirical relations between SMBH mass and host galaxy properties (e.g. Magorrian et al. 1998; Ferrarese & Merritt 2000; Gebhardt et al. 2000; Tremaine et al. 2002; Marconi & Hunt 2003; Häring & Rix 2004; Gültekin et al. 2009). Therefore, understanding the formation and evolution of the SMBH is an integral part of the current galaxy formation theory (Silk & Mamon 2012). Observationally, a first step towards understanding SMBHs is a demographic study for a wide range of black hole masses. However, it is far from complete: the number of SMBHs with a dynamical mass measurement is currently 70–80, primarily due to the difficulty of achieving the required depth and resolution (Shankar et al. 2016) and the detection of SMBHs with low (e.g. den Brok et al. 2015; Seth et al. 2010,

for $M_{BH} < 10^6$ M$_\odot$) and high (e.g. McConnell et al. 2011, for $M_{BH} > 10^{10}$ M$_\odot$) dynamical mass has rarely been reported.

Measuring the dynamical mass of SMBHs for a wide range of black hole masses and host galaxy types is required to make a robust inference of the co-evolution between the SMBH and host galaxy and also is important for calibrating other empirical methods (e.g. X-ray luminosity) of indirect mass measurements to increase the sample size of SMBHs. However, a dynamical measurement of SMBH mass is challenging due to the requirement of high angular and velocity resolution (Ferrarese & Ford 2005). Except for the rare population of galaxies with a nuclear maser (e.g. Miyoshi et al. 1995), the stellar kinematics (mostly in early-type galaxies; e.g. Kormendy 1988; Bower et al. 2001; McConnell et al. 2011) and ionized gas kinematics (in spiral and some early-type galaxies; e.g. Ferrarese, Ford & Jaffe 1996; Sarzi et al. 2001; Barth et al. 2001) have been used to measure the dynamical mass. As a result, most of the SMBH mass measurements have been obtained for a sample of early-type galaxies and spiral galaxies with a prominent bulge because they have a well-developed dynamically relaxed stellar system and powerful energy source ionizing the gas.

★ E-mail: iyoon@nrao.edu

For a comprehensive understanding of the connection between the SMBH and its host galaxy, it is important to expand the measurement of SMBH mass to the regime of small bulgeless galaxies hosting a lower mass SMBH. A recent study based on a large compilation of SMBHs shows that the empirical relation between SMBH mass and stellar velocity dispersion, known as the $M$–$\sigma$ relation (e.g. Tremaine et al. 2002), has a different normalization for early- and late-type galaxies (McConnell & Ma 2013). In addition, there is strong evidence for the low-luminosity active galactic nucleus (AGN) in bulgeless galaxies or dwarf galaxies hosting low-mass SMBHs (e.g. Filippenko & Ho 2003; Reines et al. 2011; McAlpine et al. 2011; Araya Salvo et al. 2012), whose inferred masses are largely uncertain without an accurate dynamical mass measurement. Furthermore, a large number of galaxies, presumably hosting a dust-obscured AGN (e.g. Mateos et al. 2013; Satyapal et al. 2014), has been revealed by red mid-IR colour (Stern et al. 2012). For those low-mass or dust-obscured galaxies, it may be even more difficult to apply the current methods using stellar and ionized gas kinematics if they do not have a well-developed bulge for a reliable radial velocity dispersion measurement or have dust obscuring the ionized gas, which also affects the galaxy image analysis for mass modelling.

Recently, high angular and velocity resolution radio interferometry enables us to use the observation of molecular gas kinematics to measure the dynamical mass of SMBHs (e.g. Davis et al. 2013a; Onishi et al. 2015; Barth et al. 2016). Molecular gas, as a kinematic tracer of the rotation velocity in the galactic centre, has advantages; in principle, this is possible for any galaxy type with associated molecular gas, if it exists. The high angular resolutions routinely achievable by new (sub)-millimetre interferometry (e.g. the Atacama Large Millimetre/sub-millimetre Array; ALMA) means it may be possible to probe larger volumes of the Universe than ever before, enabling a complete mass limited census of SMBHs (Davis 2014).

With the increasing importance and potential of the molecular gas kinematics for SMBH mass measurement, a figure of merit of the molecular gas kinematics has been discussed in Davis (2014), which shows that the difference between the rotation velocity with and without a SMBH can be detected by observing the molecular gas kinematics outside the black hole sphere of influence using a simple argument based on an assumed galaxy rotation velocity at a desired angular resolution of the interferometry. The required angular resolution becomes larger with decreasing concentration (measured by a logarithmic slope within 0.1 arcsec radius) of the galaxy surface brightness profile.

Although some useful formulae and discussions using galaxy samples with velocity measurement from the ATLAS$^{3D}$ survey (Krajnović 2013) have been provided in Davis (2014), their arguments are based on a single molecular gas parcel rotating around the SMBH with an assumed rotation velocity (i.e. 100 km s$^{-1}$) at the desired angular radius, without considering observational effects (e.g. beam smearing), systematic motion (e.g. non-circular motion) and the spatial distribution of the molecular gas. In addition, unlike the ATLAS$^{3D}$ survey, detailed kinematic information is not available for most galaxies, which is inconvenient for adopting the simple relation in Davis (2014) to determine the relevant physical scale for a given galaxy to resolve the gas kinematics for the SMBH mass measurement. It is useful to generalize and expand the work in Davis (2014) to the wide observing and galaxy parameter space to provide a convenient and useful guideline for estimating the angular and velocity resolution of the proposed interferometry observation without relying on prior knowledge of the galaxy rotation velocity.

Indeed, the molecular gas kinematics in a galactic centre is complicated. It is governed by the SMBH and galaxy stellar mass distribution, which is determined by the shape of the galaxy surface brightness profile, which varies for different galaxy types. Also, the signal-to-noise ratio (S/N) of the gas density profile and the profile shape, and other complicated velocity structures including inflow/outflow, random velocity motion and disc warp, may contaminate the observed molecular gas kinematics and affect our inference of the SMBH mass. We consider these effects by simulating position–velocity diagrams (PVDs) for a range of observing parameters and properties of the galaxy and the circum-nuclear molecular gas. In particular, the limits of the measurable SMBH mass given these systematic effects and the resolution of interferometry have not been discussed in detail using realistic simulations of the observed gas kinematics, which will be useful for the SMBH mass measurement using ALMA observations. In addition, it will also serve as a useful guideline for the technical justification of the ALMA proposal to observe molecular gas kinematics in galaxies for different galaxy surface brightness profiles and realistic observing conditions.

In this work, we study the parameter space of the angular and velocity resolution of radio interferometry for ranges of the galaxy types and the structure of circum-nuclear molecular gas to characterize how molecular gas kinematics can be best utilized for the SMBH mass measurement. In Section 2, we provide a simple argument to derive the relevant spatial and velocity resolution for a given galaxy surface brightness profile shape and discuss the systematic effects due to the spatial and velocity structure of the molecular gas and the effect of poor resolution of a galaxy image to determine the surface brightness profile shape and its impact on the inference of SMBH mass. In Section 3, we simulate observed PVDs and measure the rotation velocity to confirm our arguments and test the impact of systematic errors on the PVD analysis. In Section 4, we discuss the spatial resolution and velocity channel width to measure the SMBH mass as a convenient guide for the ALMA proposal. In Section 5, we summarize the results. In this work, we use the concordance LCDM cosmological model: $\Omega_m = 0.3$, $\Omega_\Lambda = 0.7$ and $H_0 = 100h$ km s$^{-1}$ Mpc$^{-1}$ where $h = 0.7$.

## 2 IMPACT OF SUPERMASSIVE BLACK HOLE ON THE ROTATION VELOCITY

To measure the SMBH mass using the gas kinematics, one needs to measure the rotation velocity accurately at the galactic centre and decompose it into two components, one from the point mass due to the SMBH and the other from the extended matter distribution due to the galaxy stellar component. The technique is not formally valid for dynamically hot, warped or inflowing/outflowing gas (Davis 2014). However, like in Davis (2014), in this section, we assume that the motion of circum-nuclear gas is purely circular and only governed by the SMBH and galaxy stellar mass, and the additional systematic effects will be discussed later.

For a flat gas disc sharing the same inclination ($i$) as the galaxy, the rotation velocity of a gas parcel at radius $r$ is

$$V(r)_{\rm rot} = \sqrt{V(r)_{\rm gal}{}^2 + \frac{GM_{\rm BH}}{r}} \sin(i) \qquad (1)$$

where $V(r)_{\rm gal}$ is the circular velocity of the galaxy due to the galaxy stellar mass distribution and $M_{\rm BH}$ is the SMBH mass in the galaxy centre.

$$V(r)_{\rm gal} = \sqrt{\frac{GM(<r)}{r}},$$

where $M(<r)$ is the enclosed mass at radius $r$ and estimated by converting the galaxy surface brightness distribution to a stellar mass distribution, using a mass-to-light ratio $(M/L)$ at the observing band. The rotation velocity $V(r)_{\rm rot}$ is then measured from the PVD.

High-resolution PVD is required to measure accurately the rotation velocity, and ALMA can easily achieve a sub-arcsec resolution that resolves the black hole sphere of influence (SOI) for most of the large SMBHs with $M_{\rm BH} > 4 \times 10^8$ M$_\odot$ and $i > 30°$ (Davis 2014), whose radius is commonly defined as

$$r_{\rm SOI} = \frac{G M_{\rm BH}}{\sigma_*^2} \qquad (2)$$

where $\sigma_*$ is the stellar velocity dispersion. Davis (2014) found that the required angular resolution to detect the effect of the black hole mass is approximately 2 times larger than $r_{\rm SOI}$ by calculating a maximum angular radius where the velocity difference with and without the SMBH is detected to be 5 times larger than the velocity channel width, using a typical galaxy rotation velocity (i.e. $V(r)_{\rm gal} = 100$ km s$^{-1}$) measured by the ATLAS$^{\rm 3D}$ survey at an assumed angular radius resolved by the Combined Array for Research in Millimeter-wave Astronomy (CARMA). However, as also mentioned in the introduction, estimating the galaxy rotation velocity as a function of the radius using more easily available photometric information is more useful and convenient for determining the angular resolution and velocity channel width for detecting the SMBH in galaxies for a wide range of morphologies without prior knowledge of the galaxy kinematics.

In practice, the observed rotation velocity $V(r)_{\rm obs}$ is different from $V(r)_{\rm rot}$ in equation (1) due to the uncertainties of the position and velocity measurements and the complicated velocity structure in the gas. However, in this section, we assume $V(r)_{\rm obs} = V(r)_{\rm rot}$ by neglecting the complicated velocity structure and simplifying the uncertainties in the PVD by considering only the interferometry beam size and velocity channel width. We consider other systematic effects by simulating PVDs in Section 3.4.

### 2.1 Rotation velocity

We compute $V(r)_{\rm rot}$ using $M_{\rm BH}$ and $V(r)_{\rm gal}$ in equation (1). To compute $V(r)_{\rm gal}$, we adopt Sérsic models for the galaxy surface brightness profile to estimate the enclosed mass at a radius $r$. The surface brightness profile of a Sérsic model (Sersic 1968) varies with a shape parameter $n$ and produces a profile continuously changing from disc to elliptical galaxies. It is also possible to extend the Sérsic model to incorporate a core-deficit of elliptical galaxies by using a core-Sérsic model (e.g. Graham et al. 2003). Although in practice the galaxy surface brightness profile is measured from a high-resolution galaxy image with additional modelling of the details of the profile such as a nuclear star cluster (e.g. Emsellem, Monnet & Bacon 1994), we use the Sérsic parametric model in this study because it is flexible in describing a wide range of galaxy surface brightness profiles very well and thus effective to show the impact of the galaxy surface brightness profile shape on the SMBH mass measurement.

The surface brightness profile of the Sérsic model is

$$I(r) = I(0) \exp[-b_n (r/r_{\rm es})^{1/n}] \qquad (3)$$

with $I(0)$ being the central intensity, $r_{\rm es}$ the half-light radius and $n$ the shape parameter.

The surface brightness profile of the core-Sérsic model is

$$I(r) = I_b \left[ \left(\frac{r_b}{r}\right)^\gamma u(r_b - r) + e^{b(r_b/r_e)^{1/n} - b(r/r_e)^{1/n}} u(r - r_b) \right] \qquad (4)$$
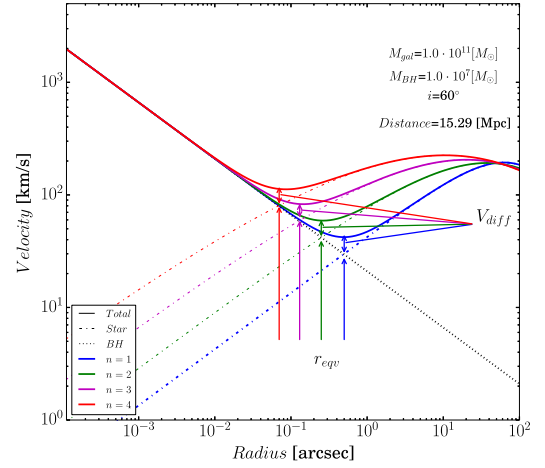


**Figure 1.** Rotation velocity of a galaxy with $M_* = 10^{11}$ M$_\odot$ containing a central SMBH with $M_{\rm BH} = 10^7$ M$_\odot$. Different colours indicate the Sérsic index of the galaxy. Keplerian rotation due to the SMBH is shown by the black dotted line and rotation velocity due to the galaxy stellar mass is shown by the dot-dashed line. The solid line is the total rotation velocity. The radius, where the galaxy rotation and the SMBH rotation velocity are equal ($r_{\rm eqv}$) for each galaxy surface brightness profile, is indicated by the arrow with the same colour as the corresponding rotation curve. The velocity difference $V_{\rm diff}$ between the total (galaxy + SMBH) and galaxy rotation velocity at $r_{\rm eqv}$ is also shown by the arrow with the same colour scheme.

with $u(r-a)$ being the Heaviside step function for a sharp transition at $r_b$ (Trujillo et al. 2004). Although this is different from the original core-Sérsic model profile (Graham et al. 2003), replacing $b$ with $b_n$ and half-light radius $r_e$ with that of the outer Sérsic profile $r_{\rm es}$ gives a good approximation with much less error than the uncertainty in $r_e$ from the fitting process as long as $r_b \ll r_e$ (Trujillo et al. 2004). So in this work, we use equation (4) for the core-Sérsic galaxy model.

To compute the enclosed mass within $r$, we integrate $I(r)$ up to $r$. This is normalized by the total luminosity $\int_0^\infty I(r) \mathrm{d}r$. Then we multiply by the bolometric luminosity and mass-to-light ratio. We use a fiducial mass-to-light ratio, $M/L = 1.0$ and adjust an absolute magnitude parameter to obtain the galaxy stellar mass that we want to control. Given galaxy stellar mass $M_*$ and Sérsic index $n$, we assign the half-light radius of the galaxy using the relation in Shen et al. (2003):

$$\frac{r_{\rm es}}{\rm kpc} = \begin{cases} 0.1 \left(\frac{M_*}{\rm M_\odot}\right)^{0.14} \left(1 + \frac{M_*}{3.98 \times 10^{10}\,\rm M_\odot}\right)^{0.25}, & \text{if } n < 2.5, \\ 2.88 \times 10^{-6} \left(\frac{M_*}{\rm M_\odot}\right)^{0.56}, & \text{if } n > 2.5. \end{cases}$$

$$(5)$$

If the galaxy stellar mass $M_*$ and Sérsic index $n$ are given, the enclosed stellar mass $M_*(<r)$ is

$$M_*(<r) = M_* \frac{\int_0^r I(r)\mathrm{d}r}{\int_0^\infty I(r)\mathrm{d}r} = M_* \frac{\gamma(2n, x)}{\Gamma(2n)} \qquad (6)$$

where $x = b_n (r/r_{\rm es})^{1/n}$. For $n > 0.36$, $b_n$ is approximated as (Ciotti & Bertin 1999):

$$b_n \approx 2n - \frac{1}{3} + \frac{4}{405n} + \frac{46}{25\,515n^2} + \frac{131}{1148\,175n^3} - \frac{2194\,697}{30\,690\,717\,750n^4} + O(n^{-5}). \qquad (7)$$

Fig. 1 shows the rotation velocity of a galaxy with inclination $i = 60°$ and $M_* = 10^{11}$ M$_\odot$ containing a $10^7$ M$_\odot$ SMBH for
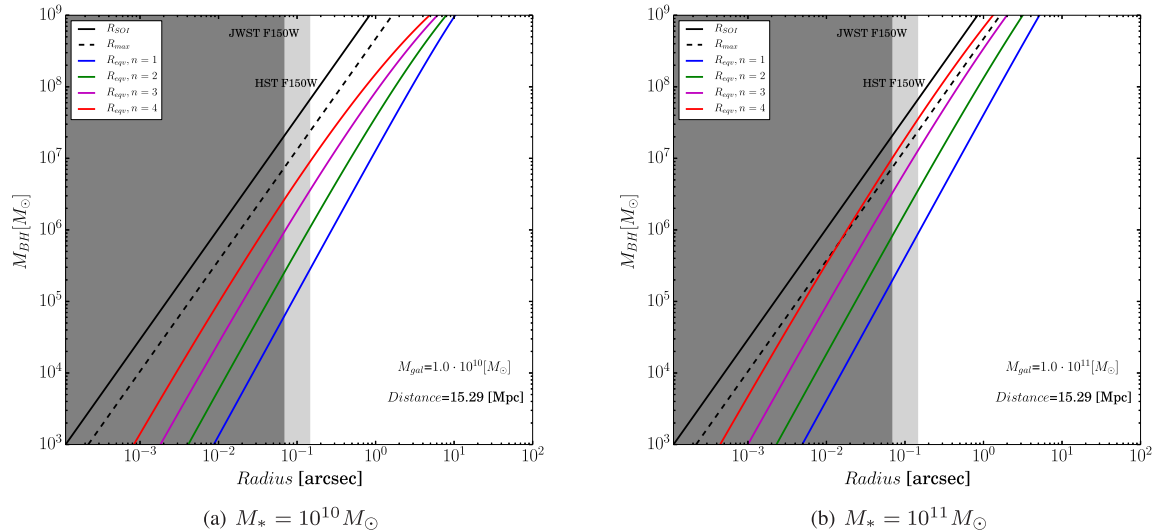
**Figure 2.** Relation between SMBH mass and the three different angular scales, $r_{\rm SOI}$, $r_{\rm max}$ and $r_{\rm eqv}$ for a given galaxy stellar mass $M_*$. For $r_{\rm SOI}$, we combine equation (2) and a recent compilation of the $M$–$\sigma$ relation (McConnell & Ma 2013). For $r_{\rm max}$, we use the best-fitting relation between $r_{\rm SOI}$ and $r_{\rm max}$ ($r_{\rm max} = 1.92 r_{\rm SOI}$) in Davis (2014). For $r_{\rm eqv}$, different colours indicate galaxy surface brightness profiles characterized by different Sérsic indices $n$.

different surface brightness profile shapes characterized by Sérsic index $n$. For the $x$-axis, we use the angular size at a given luminosity distance of the galaxy (roughly at the distance of the Virgo cluster, $\approx 15$ Mpc) instead of physical size for easy comparison with the angular resolution of ALMA. Each colour in Fig. 1 represents a Sérsic index, ranging from 1 to 4. The rotation velocity, shown by the solid lines, is decomposed into the rotation velocity due to the SMBH and the galaxy stellar mass distribution. The dotted lines and dot–dashed lines are the rotation velocities due to the SMBH mass and galaxy stellar mass, respectively. We also annotate the angular radius $r_{\rm eqv}$ where the rotation velocity due to the SMBH and due to the galaxy stellar mass distribution become equal [i.e. $M_* \gamma(2n, x)/\Gamma(2n) = M_{\rm BH}$], and we indicate the velocity difference $V_{\rm diff}$ at $r_{\rm eqv}$ between the total rotation velocity and the rotation velocity due to the galaxy stellar mass. If the beam size is larger than $r_{\rm eqv}$ or the velocity channel width is larger than $V_{\rm diff}$ for the given beam size resolving $r_{\rm eqv}$, the velocity difference $V_{\rm diff}$ is not resolved. So, $r_{\rm eqv}$ and $V_{\rm diff}$ determine the required beam size and velocity channel width $\Delta V$ [defined as $\Delta V = (1/3)V_{\rm diff}$ for detecting $V_{\rm diff}$ at $3\sigma$] of the radio interferometry.

Fig. 1 indicates that at fixed galaxy stellar mass, the impact of Keplerian motion due to the SMBH extends to a larger radius as the galaxy surface brightness profile becomes less concentrated (i.e. with a smaller Sérsic index). For example, the rotation velocity due to the SMBH at 0.5 arcsec scale is 5 times smaller than that due to the galaxy stellar mass if the galaxy surface brightness profile follows that of elliptical galaxies ($n = 4$ shown by the red curve) while the rotation velocity due to the SMBH is the same as the rotation velocity due to the galaxy stellar mass at the same 0.5 arcsec angular scale if the surface brightness profile is exponential ($n = 1$ shown by the blue curve). This implies that the effect of the SMBH for fixed mass $M_{\rm BH}$ can be detected by a larger angular resolution as the galaxy surface brightness profile becomes less concentrated, which is consistent with the finding in Davis (2014). On lowering the SMBH mass, the dotted line moves downwards and thus, for fixed angular resolution, the $r_{\rm eqv}$ of a larger Sérsic index galaxy starts to be unresolved. This implies that the effect of SMBH for a given galaxy stellar mass and angular resolution can be more easily detected for a lower black hole mass if the galaxy surface brightness

profile becomes less concentrated. This will be discussed further in the following section.

## 2.2 Spatial and velocity resolution

The radius $r_{\rm max}$ defined in Davis (2014) as where the Keplerian motion due to the SMBH shows a statistically significant deviation from the rotation velocity due to the galaxy stellar mass distribution is larger than the black hole sphere of influence $r_{\rm SOI}$ (equation 2). Using galaxy samples in ATLAS$^{\rm 3D}$, Davis (2014) found that $r_{\rm max} = 1.92 r_{\rm SOI}$ at a $5\sigma$ statistical significance level.

For a given $M_{\rm BH}$, we compare three different radii, $r_{\rm SOI}$, $r_{\rm max}$ and $r_{\rm eqv}$, for galaxies with the same stellar mass with different surface brightness profiles. The black hole $r_{\rm SOI}$ is computed by combining equation (2) and the relation between the SMBH mass and the stellar velocity dispersion in McConnell & Ma (2013). Fig. 2 shows these radii (i.e. angular sizes for a given galaxy distance) for a range of SMBH masses for a galaxy with $M_* = 10^{10}$ M$_\odot$ (Fig. 2a) and $M_* = 10^{11}$ M$_\odot$ (Fig. 2b). The solid black line is $r_{\rm SOI}$, the dashed black line is $r_{\rm max}$ and the coloured solid lines are $r_{\rm eqv}$ for different Sérsic indices ($n = 1, 2, 3$ and $4$). The following relation provides a convenient way to determine $r_{\rm eqv}$ for a given ratio between the SMBH mass and the galaxy stellar mass:

$$\frac{M_{\rm BH}}{M_*} = \frac{\gamma(2n, x)}{\Gamma(2n)}, \tag{8}$$

where $x = b_n (r/r_{\rm es})^{1/n}$ and $b_n$ is estimated by equation (7). The region smaller than the full width at half-maximum (FWHM) of *Hubble Space Telescope* (HST) WFC3 (0.15 arcsec)[1] and *James Webb Space Telescope* (JWST) NIRCam (0.068 arcsec)[2] in the $J$ band are shown by light and dark grey areas to show the limit of angular resolution beyond which the galaxy surface brightness profile can be accurately measured using a high-resolution near-infrared image. Although a current state-of-the-art resolution image for SMBH mass

---

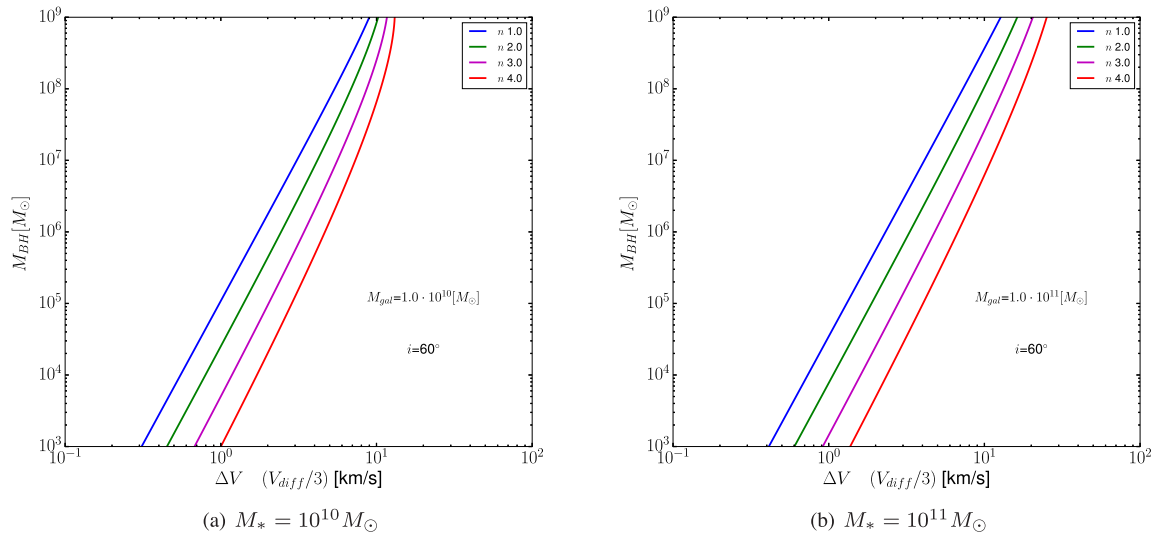[1] http://www.stsci.edu/hst/wfc3/documents/handbooks/currentIHB/c07_ir07.html

[2] http://www.stsci.edu/jwst/instruments/nircam/PSFs/

**Figure 3.** Same as Fig. 2, but for the velocity channel width $\Delta V$.

measurement using a HST/ACS *I*-band image has slightly smaller FWHM ($\approx 0.1$ arcsec), the important question is whether the very inner region, where the rotation velocity is dominated by the SMBH, is resolved both by the photometric point spread function (PSF) and the interferometer beam or not, and therefore, the actual size of the FWHM is not relevant for the discussion in this section.

In Fig. 2, for all galaxy profiles, $r_{eqv}$ is larger than $r_{SOI}$. All colour solid lines, except for the galaxy with $n = 4$, $M_* = 10^{11}$ M$_\odot$ and $M_{BH} > 10^6$ M$_\odot$, are larger than $r_{max}$ by a factor of a few for the galaxy with $n = 4$ and by more than an order of magnitude for the galaxy with $n = 1$, and this deviation becomes larger for lower SMBH mass. The best agreement between $r_{max}$ and $r_{eqv}$ is seen for the galaxy with $M_* = 10^{11}$ M$_\odot$ and $n = 3$–4 for $M_{BH} > 10^7$ M$_\odot$, which is like the galaxies in Davis (2014) used for deriving $r_{max}$. However, $r_{max}$ was determined for $5\sigma$ statistical significance (Davis 2014) and, thus, $r_{max}$ can be larger by a linear factor of the inverse of the significance level for a small velocity error (i.e. channel width) compared with the rotation velocity (see equation 9 in Davis 2014), on lowering the significance level. As the galaxy surface brightness profile becomes less concentrated, the required beam size for detecting the SMBH becomes larger at fixed $M_{BH}$ and the detectable SMBH mass becomes smaller at fixed beam size. This is an advantage for detecting a lower mass black hole residing in a small bulgeless galaxy.

In the same manner, we also show the velocity channel width $\Delta V$ [$=(1/3)V_{diff}$] for different SMBH masses, for a galaxy with $M_* = 10^{10}$ M$_\odot$ (Fig. 3a) and $M_* = 10^{11}$ M$_\odot$ (Fig. 3b). The observed rotation velocity depends on galaxy inclination ($i$) and we assume $i = 60°$ in Fig. 3. The required velocity channel width for detecting the SMBH becomes smaller at fixed $M_{BH}$ and the detectable SMBH mass becomes larger at fixed velocity channel width, as the galaxy surface brightness profile is less concentrated. This is a disadvantage for a small bulgeless galaxy. However, the range of variation of the velocity channel width for different galaxy Sérsic indices is within a factor of a few, which is much smaller than the variation of the angular resolution (i.e. an order of magnitude) and ALMA has sufficient velocity resolution ($\leq 1$ km s$^{-1}$) to cover the range of this channel width in Fig. 3. So, the practical benefit is the spatial resolution. However, we note that the small velocity channel width does not improve the significance of the detection if the velocity uncertainty including the systematic and random

motion is larger than the velocity channel width, as also noted by Davis (2014).

### 2.3 Effects of spatial and velocity structure of molecular gas

The above argument regarding the spatial and velocity resolution aplies for rotating molecular gas following the gravitational potential from the central SMBH and the galaxy stellar mass. In a realistic situation, we need to understand how significant the effects of the spatial and velocity structure of the molecular gas are on the observed rotation velocity. It is not trivial to quantify how these systematic effects influence the detection of the SMBH mass using analytic arguments. However, we will qualitatively discuss their effects here and show their significance using simulations of the PVD in Section 3.4.

First, we consider the systematic effect due to the spatial distribution of the molecular gas. Recent ALMA observations have revealed the detailed structure of molecular gas at a 10–100 pc scale. Most of them show a disc-like morphology with and without a hole at the centre (e.g. Izumi et al. 2013; Combes et al. 2014; Onishi et al. 2015; Xu et al. 2015). If the gas distribution is continuous and smooth, the central region of the PVD is sampled well and the impact of the SMBH on the rotation velocity, if significant, can be detected. However, if the molecular gas distribution has a hole at the centre and the size of the hole is larger than $r_{eqv}$, there will be no velocity tracers at the centre and the PVD analysis will not probe the region with the largest statistical significance in the velocity space for detecting the SMBH. In addition, for the same background noise and the same amount of total flux from the molecular gas, if the gas profile shape in the central region is homogeneous across many synthesized beams, a peak flux at the centre where the impact of the SMBH mass is observed the most becomes relatively low and the signature of the SMBH will be less significant than that for molecular gas with a more concentrated profile, which implies that the gas disc profile shape might affect the uncertainty of the rotation velocity measurement and the resulting SMBH mass. Since the proposed sensitivity requirement of ALMA is defined per beam, the flux variation due to the spatial geometry of the gas disc within the ALMA beam may impact the modelling of the gas kinematics given that the geometry of the circum-nuclear molecular gas is not known a priori. Also, if the geometry of the molecular gas disc becomes
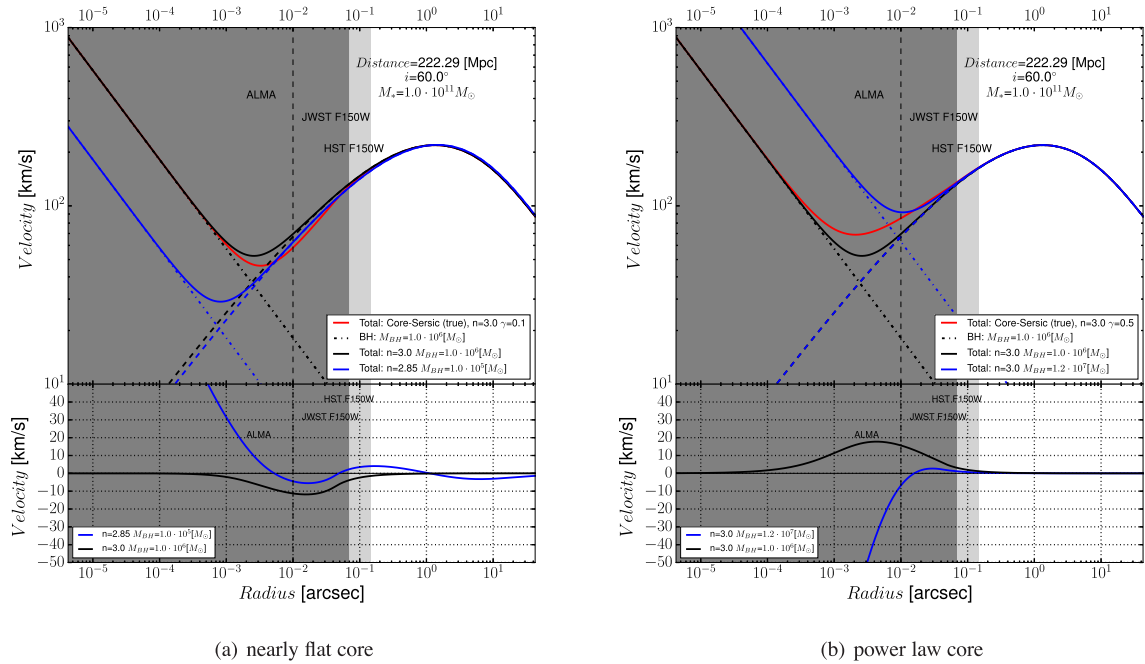
(a) nearly flat core            (b) power law core

**Figure 4.** Rotation velocity of a galaxy with $M_* = 10^{11}$ M$_\odot$ containing a $10^6$ M$_\odot$ SMBH. The surface brightness profile of the galaxy is the core-Sérsic profile with $r_b = 0.01 r_e$ and $n = 3$ in equation (4). (a) The galaxy has a nearly flat core ($\gamma = 0.1$). The red line shows the total rotation velocity of the true galaxy model including the SMBH. The black line shows the rotation velocity of the same galaxy with the same Sérsic index and the same SMBH mass but without the core. The blue line is the rotation velocity of the Sérsic model galaxy (without a core) with 5 per cent smaller Sérsic index (i.e. $n = 2.85$) and 3 per cent larger mass-to-light ratio (i.e. $M/L = 1.03$) than the galaxy shown by the black line, however, with a 10 times smaller SMBH mass ($10^5$ M$_\odot$) than the true value ($10^6$ M$_\odot$). (b) The galaxy has a core with power-law profile ($\gamma = 0.5$). The red and black lines indicate the same case in panel (a). The blue line is the rotation velocity of the Sérsic model galaxy (without a core) with the same Sérsic index (i.e. $n = 3.0$) and mass-to-light ratio (i.e. $M/L = 1.0$) as the galaxy shown by the black line, however, with a 12 times more massive SMBH mass ($1.2 \times 10^7$ M$_\odot$) than the true value ($10^6$ M$_\odot$).

closer to face-on, the projected line-of-sight velocity decreases and a smaller velocity channel width is required to resolve the velocity difference between the pure galaxy rotation and the galaxy-SMBH rotation. In contrast, if the galaxy is edge-on and the beam size is too large to resolve the kinematic structure along the minor axis, the velocity profile smears due to the velocity components migrated from the minor axis (Barth et al. 2016). Another potential problem is a warp in the gas disc. A warp is prominent in the H I distribution (e.g. García-Ruiz, Sancisi, & Kuijken 2002) but is also seen in a nuclear molecular gas disc (Sofue & Rubin 2001). It introduces a bias in the inclination correction and underestimates the rotation velocity depending on the location of the major axis (Vergani et al. 2003), which can be mitigated by modelling the full 3D data cube.

Secondly, we consider the systematic effect due to the velocity structure of molecular gas. In reality, the velocity structure of molecular gas is more complicated than pure circular motion. This velocity structure, which we call non-circular motion in this work, includes the gas inflow due to angular momentum loss (e.g. Combes et al. 2014) and the gas outflow due to strong stellar and AGN feedback (e.g. García-Burillo et al. 2014), both of which have been observed by ALMA. For a set of molecular gas parcels within the radio beam along the line of sight at a certain projected distance, this bulk motion (inflow or outflow) contributes to the line-of-sight velocity of the gas parcels positively or negatively depending on where the gas parcels are located. This will cause a velocity spread in the PVD and, at a given radius, make the PVD thicker along the velocity axis. As a result, the signature of Keplerian rotation owing to the SMBH will not be significant. Although the driving mechanisms are different, both inflow and outflow have the same effect

on the PVDs, with the only difference being the velocity sign. In addition, there is a random motion in the circum-nuclear molecular gas, which also introduces a dispersion in the velocity axis in the PVD.

### 2.4 Galaxy surface brightness profile bias

To measure the SMBH mass using the rotation velocity of the circum-nuclear molecular gas, the surface brightness profile at the galactic core needs to be accurately determined (e.g. Ferrarese & Ford 2005), which requires a high angular resolution to resolve $r_{\rm eqv}$. However, the angular resolution of the galaxy image may not be sufficient to characterize the core luminosity profile accurately for distant galaxies while radio interferometry still has sufficient resolution to resolve $r_{\rm eqv}$.

A detailed analysis of the high-resolution HST images of early-type galaxies reveals that the galaxy core surface brightness profiles deviate from the Sérsic model fit and have a flat core or a power-law slope (e.g. Trujillo et al. 2004) although the Sérsic model is a good fit to the overall profile in general (e.g. Caon, Capaccioli & D'Onofrio 1993; Graham 2001). If the galaxy core profile is not resolved, the stellar mass distribution at the galactic centre is systematically biased and, as a result, the derived rotation velocity is also biased. This bias introduces a large systematic error in the SMBH mass measurement. In Section 3.5, we illustrate how the bias in the galaxy surface brightness profile can impact the SMBH mass measurement.

In Fig. 4, we show the rotation velocity of a galaxy with a SMBH using a core-Sérsic galaxy surface brightness profile with the core

being unresolved by putting this galaxy at large distance such that, at the scale of the HST and JWST seeing, the galaxy rotation velocity is largely dominated by the galaxy stellar mass distribution (not by the SMBH) and the difference between the rotation velocities due to the slightly different surface brightness profiles of the galaxy cannot be discriminated. The core-Sérsic galaxy has $M_* = 10^{11}$ $M_{\odot}$ and $M_{BH} = 10^6$ $M_{\odot}$, and follows the surface brightness profile with Sérsic index $n = 3$ and core radius $r_b = 0.01r_e$ ($r_b \ll r_e$ in equation 4). We consider two different core profiles: a nearly flat core using $\gamma = 0.1$ and a power-law core using $\gamma = 0.5$ (see equation 4), representing the typical values for elliptical galaxies seen in Trujillo et al. (2004).

Figs 4(a) and (b) show the rotation velocities due to different galaxy surface brightness profiles and SMBH masses and their residuals from the true rotation velocity. As in Fig. 2, the region smaller than the PSF FWHM for HST WFC3 and JWST NIRCam is shown by light and dark grey areas, respectively. The highest angular resolution of ALMA ranges from 0.006 arcsec at 675 GHz to 0.037 arcsec at 110 GHz. We assume a 0.01 arcsec beam size as a typical ALMA resolution for the most extended array configuration and show it by a vertical dashed line in Fig. 4.

In the upper panels of Figs 4(a) and (b), we show three different rotation velocities. First, the red lines show the true rotation velocity of the core-Sérsic galaxy with a nearly flat core ($\gamma = 0.1$, Fig. 4a) and a power-law core ($\gamma = 0.5$, Fig. 4b). Secondly, the black lines show the rotation velocity of the galaxy that follows the surface brightness profile with the same $n$ as the core-Sérsic galaxy and the same SMBH mass but without the core. Last, the blue lines are for a galaxy rotation velocity that shows better agreement with the true rotation velocity (red) for a scale larger than the ALMA angular resolution, by using very small (or no) adjustment of the Sérsic index and mass-to-light ratio while using an order of magnitude different SMBH mass. In detail, the blue line in Fig. 4(a) shows the case where the galaxy has a 5 per cent smaller Sérsic index ($n = 2.85$) and a 3 per cent larger mass-to-light ratio ($M/L = 1.03$) than the true values but has a 10 times smaller SMBH mass ($10^5$ $M_{\odot}$). The blue line in Fig. 4(b) shows the case where the galaxy has the same Sérsic index ($n = 3.0$) and mass-to-light ratio ($M/L = 1.0$) as the model galaxy shown by the black line, but has a 12 times more massive SMBH ($1.2 \times 10^7$ $M_{\odot}$).

In the lower panels of Figs 4(a) and (b), we show the residual velocities from the true rotation velocity (red curves in the upper panels), for the model galaxies in the upper panels using the same colours. For both cases of the biased galaxy surface brightness profile with largely biased SMBH mass that shows a better agreement with the true rotation velocity, the velocity difference at an angular scale larger than the assumed ALMA resolution (0.01 arcsec) is smaller than the typical velocity channel width adopted for measuring the SMBH mass using molecular gas kinematics (e.g. 10 km s$^{-1}$ in Davis et al. 2013a) and their velocity residual at the spatial scale resolved by HST and ALMA is smaller than the velocity residuals of the galaxy with the same global Sérsic index as the core-Sérsic galaxy (blue lines).

The rotation velocity of the true core-Sérsic galaxy (red line) and the same Sérsic galaxy profile without a core (black line) are indistinguishable at the scale of the HST and JWST resolution ($\approx 0.1$ arcsec) with a 1–2 km s$^{-1}$ velocity difference as seen by the black lines in the lower panels of Figs 4(a) and (b). Therefore, if the core of the galaxy surface brightness profile is not resolved, the Sérsic galaxy profiles with the unresolved core (black lines in the upper panels of Fig. 4) may be the best determination of the galaxy stellar mass distribution. However, the rotation velocity of

this biased profile is not a good match to the true rotation velocity of the core-Sérsic galaxy at an angular scale like the ALMA beam (0.01 arcsec). The blue line with slightly adjusted galaxy parameters ($n$ and $M/L$) but with an order of magnitude different black hole mass is a better match to the true rotation curve at the angular resolution of ALMA. This results in a biased SMBH mass in model fitting, as demonstrated in Section 3.5.

Lowering the ALMA resolution to less than 0.01 arcsec in this example will remove the bias; however, achieving 0.01 arcsec resolution is very difficult (if not feasible) in practice for many galaxies because of the long integration time. So for nearby galaxies, ALMA has sufficient spatial resolution to resolve $r_{eqv}$ and, thus, even though the galaxy rotation velocity is biased due to the unresolved galaxy core in the photometric image, ALMA can distinguish the difference between slightly different galaxy rotation velocities. However, for distant galaxies, the ALMA spatial resolution becomes poor and cannot differentiate the velocities due to the biased galaxy surface brightness profiles. This implies that at the current best ALMA resolution, it is difficult to break the degeneracy between different rotation velocities due to the biased core surface brightness profiles not resolved by HST or JWST, if the galaxy is at a distance similar to or larger than $\approx 200$ Mpc. In principle, to avoid the bias of the SMBH mass owing to the biased galaxy surface brightness profile, the resolution of the galaxy image should be like the ALMA beam size and ideally, both need to be comparable to $r_{eqv}$ assuming that a sufficient velocity resolution is achieved by ALMA.

## 3 DETECTING THE IMPACT OF A SMBH

We have discussed the angular and velocity resolution required to measure the impact of a SMBH based on the rotation velocity without considering the observational measurement processes. We argue that if the galaxy stellar mass, surface brightness profile shape and inclination are known, there is a required spatial resolution corresponding to $r_{eqv}$ and velocity channel width corresponding to $(1/3)V_{diff}$ to detect the SMBH mass that one aims to measure. In this section, we confirm this argument and show how the angular resolution and velocity channel width affect the SMBH mass detection by simulating PVDs with a model rotation velocity including the observational measurement processes. Then we incorporate the systematic effects in the PVD simulation to test how significant their impacts are on the measurement of the rotation velocity for several representative cases.

### 3.1 Simulations of the position–velocity diagram

We use KINMS (Davis et al. 2013b) to simulate the PVD. KINMS[3] is publicly available Interactive Data Language (IDL) code used to simulate gas kinematics by incorporating the observational effects (beam size and velocity channel width) and the properties of the molecular gas [user-defined gas density profile, random velocity dispersion, bulk motions (inflow/outflow), warp and blobs in the molecular gas]. Although it was originally developed to model the gas kinematics in elliptical galaxies in the ATLAS$^{3D}$ survey (Davis et al. 2013b), it is also directly applicable to the analysis of molecular gas kinematics for SMBH mass measurement (Davis et al. 2013a; Onishi et al. 2015). For detailed information about the code, refer to Davis et al. (2013b).
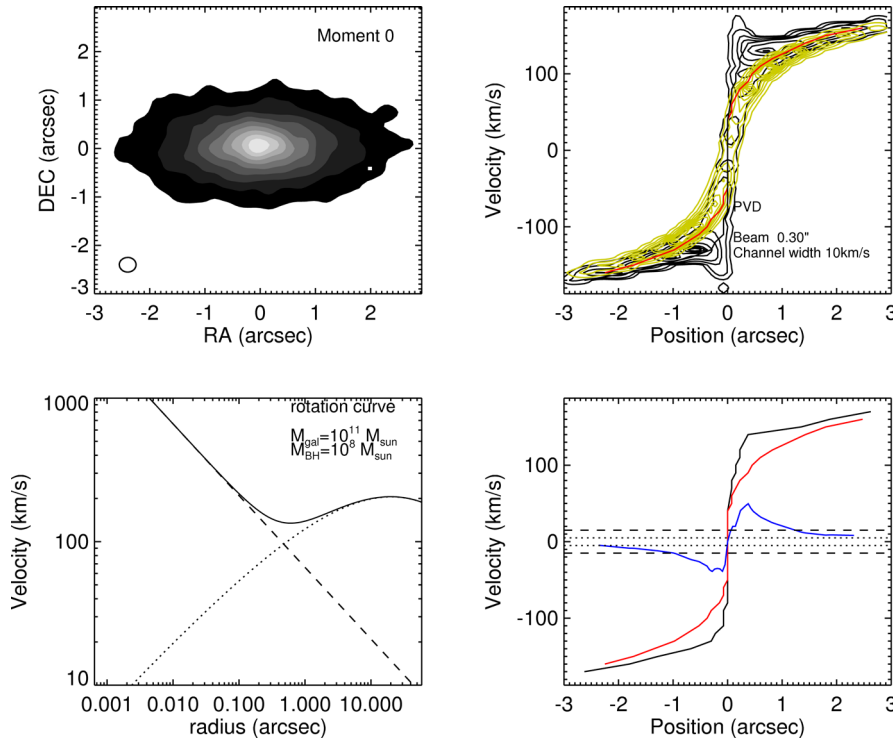
---

[3] https://github.com/TimothyADavis/KinMS

**Figure 5.** PVD simulation with S/N = 100 for a galaxy with $M_* = 10^{11}$ M$_\odot$ $i = 60°$, $n = 3$ and $M_{BH} = 10^8$ M$_\odot$. We assume a simple exponential disc with a scale radius of 1 arcsec for the molecular gas, which has the same inclination angle as the galaxy. A 0.3 arcsec beam size and 10 km s$^{-1}$ velocity channel width is used to generate this PVD. The top left-hand panel shows the integrated line intensity map and the top right-hand panel shows the simulated PVD for the galaxy stellar mass (yellow) on top of the PVD of the entire system (black: galaxy and SMBH). The lower left-hand panel shows the input rotation velocity used to generate this PVD and the lower right-hand panel shows the rotation velocities measured from the PVD (black for the entire system and red for the galaxy without the SMBH) and the residual of the two rotation velocities (blue line). The dashed and dotted lines are the 3 and 1$\sigma$ significances for the residual rotation velocity, defined by 3 $\times$ and 1 $\times$ the velocity channel width.

In a PVD simulation, we generate the noise as follows. We sample the spatial distribution of the molecular gas using a finite number of random samples to make the PVD. After sampling the distribution 100 times using different random numbers, we estimate the standard deviation of the ensemble PVDs from a noise-less PVD generated from the density distribution sampled by a large number ($10^6$) of random samples. Then the S/N of the PVD is defined by the peak signal in the PVD and the standard deviation of the ensemble PVDs. We vary the number of random samples ($N_{\rm samp}$) to obtain a range of S/N values in this work. However, S/N not only depends on the number of random samples but also on the beam size, velocity channel width and pixel resolution; the larger the values, the larger the S/N for the same number of random samples. We find that for most of our experiments in this work, approximately 10 000 random samples gives a good S/N ranging from 60 to 100. However, we note that the real noise in a PVD originates from spatially correlated interferometer noise and, thus, depends on the spatial scale of the observation. This requires a more complicated simulation of the PVD using a realistic array configuration, which is beyond the scope of the current work.

Fig. 5 shows a simulation of a $10^{11}$ M$_\odot$ galaxy with $n = 3$ and $i = 60°$ containing a $10^8$ M$_\odot$ SMBH at $\approx 15$ Mpc distance. The required beam size ($r_{\rm eqv}$) and velocity channel width [$(1/3)V_{\rm diff}$] for this galaxy are 0.5 arcsec and 12 km s$^{-1}$ based on the discussion in Section 2.2. The molecular gas distribution around the SMBH is simply assumed to be an exponential disc with a 1 arcsec scale radius and the same inclination angle as the galaxy. The peak S/N is $\approx 100$ using 10 000 random samples.

The top left-hand panel shows the velocity-integrated flux distribution (i.e. moment 0 map) with 0.3 arcsec beam. The top right-hand panel shows the PVD of the galaxy using a 0.3 arcsec beam size and 10 km s$^{-1}$ velocity channel width. We use a slightly smaller beam size and velocity channel width than the required values (0.5 arcsec and 12 km s$^{-1}$) to give a clear demonstration of the impact of the SMBH. Yellow contours on top of the background black contours are the PVD due to the galaxy stellar mass without the SMBH and the background black contours are the PVD for the entire system (galaxy and SMBH). The lower left-hand panel shows the input rotation velocity used to generate the PVD showing the contribution from the SMBH and the galaxy stellar mass distribution. The lower right-hand panel shows the rotation velocity of the galaxy with and without the SMBH measured from the PVD and the difference between the two velocities is the blue line accompanied by the 3$\sigma$ and 1$\sigma$ level velocity uncertainties (defined by 3 $\times$ and 1 $\times$ velocity channel widths) as shown by the dashed and dotted lines.

Rotation velocities are derived from the yellow and black contours using envelope-tracing methods (Sofue & Rubin 2001), which use the terminal velocity in the PVD along the major axis. The terminal velocity is defined as the velocity at which the intensity becomes equal to $I_t = \sqrt{(\eta I_{\rm max})^2 + I_{\rm lc}^2}$ on the PVD, where $I_{\rm max}$ and $I_{\rm lc}$ are the maximum intensity and the intensity corresponding to the lowest contour level. Using $\eta = 0.5$, this defines a velocity at the 50 per cent level of the intensity profile at a fixed position for sufficiently large S/N or a velocity along the lowest contour level if the S/N is small (Sofue & Rubin 2001). This will capture the circular velocity that lies at the outer envelope of the PVD.

We caution that the velocity determined by tracing the outer envelope of the PVD is biased towards the material along the line of sight and does not trace very well the Keplerian rise in the PVD seen in Fig. 5. Some of the issues discussed in this section can be removed by fitting the 2D PVD intensity map itself or the entire 3D data cube. A detailed comparison of the performance of different methods is beyond the scope of this work. However, we note that our approach in tracing the outer envelope of the PVD is conservative and, therefore, it ensures that more sophisticated fitting methods will provide a better constraint to the SMBH mass.

For illustration, we select a typical example of an SMBH and a host galaxy. The assumed SMBH mass ($10^8$ M$_\odot$) and galaxy stellar mass ($10^{11}$ M$_\odot$) are not in the extreme range (e.g. a dynamically measured $10^{10}$ M$_\odot$ SMBH in an $10^{11}$ M$_\odot$ galaxy was reported by van den Bosch et al. 2012). In the upper right-hand panel of Fig. 5, we are able to detect a signature of the SMBH as revealed by the high-velocity tip of the black contour at the centre, which is indicative of Keplerian rotation. Looking at the residual rotation velocity shown by the blue line in the lower right-hand panel of Fig. 5, the maximum deviation at the centre is much larger than the $3\sigma$ velocity uncertainty and the deviation is larger than the $1\sigma$ range for the entire range of the spatial scale. In this case, it is relatively easy to claim a detection of the SMBH mass. However, for a given $M_{BH}$ and galaxy stellar mass, the significance of this deviation will be smaller with increasing beam size and velocity channel width of the radio interferometry. Since it is already obvious that an SMBH with large enough mass will be easily detected, as shown in this example, we will test the case of the lowest detectable SMBH masses for the given galaxy parameters inferred from Figs 2 and 3.

## 3.2 Effect of noise

Before we investigate the impact of the systematic effect on the PVD analysis, we discuss the effect of noise. We take a fiducial galaxy with $M_* = 10^{11}$ M$_\odot$ including the SMBH with $M_{BH} = 10^7$ M$_\odot$ of which the surface brightness follows a Sérsic profile with $n = 3$ and $i = 60°$. Then we assume that the gas surface density distribution is an exponential disc with a 1 arcsec scale radius and sample the density distribution using a finite number of random samples as discussed above. For this galaxy, the minimum required beam size and velocity channel width are 0.15 arcsec and 8 km s$^{-1}$, respectively, as inferred from Figs 2 and 3. For this beam size and channel width, we make PVDs with four different signal-to-noise ratios: S/N = 10, 30, 60 and 120 determined by 150, 1400, 6000 and 24 000 random samples, respectively. Note that S/N is roughly proportional to $\sqrt{N_{samp}}$ as expected from statistics.

Fig. 6 shows the rotation velocity of the galaxy with the SMBH (black), without the SMBH (red) and the residual velocity between the two (blue). For each S/N, we generate 100 ensemble PVDs and each solid line with error bars is the mean of these ensemble measurements with the standard deviations of the ensemble PVDs. When the S/N is low (10), both the black and red lines have large errors and, thus, the residual velocity is largely uncertain; the standard deviation in the central region is larger than $3\Delta V$. As S/N increases, the uncertainty of the rotation velocity measurement becomes smaller. When S/N = 60, it becomes much smaller than $\Delta V$ in the outer region and comparable to the $\Delta V$ in the centre. This noise simulation confirms our intuition that the rotation velocity difference with and without the SMBH becomes less significant as S/N decreases and it will increase the uncertainty of the SMBH mass measurement.

In the following experiments to investigate the required spatial and velocity resolution (Section 3.3) and to demonstrate the impact of systematic effects on the PVD analysis (Section 3.4), we ensure that the PVD has a reasonably good S/N ($\approx$60) by choosing the appropriate number of random samples for a given beam size and velocity channel width for each experiment.

## 3.3 Spatial and velocity resolution

In Fig. 7, we simulate PVDs of the same galaxy (i.e. the galaxy in Fig. 6 with $M_* = 10^{11}$ M$_\odot$, $M_{BH}=10^7$ M$_\odot$ and $i = 60°$) for four different Sérsic indices ($n = 1, 2, 3$ and 4) and investigate the significance of the difference between the rotation velocities of the galaxy with and without the SMBH, using different beam sizes and velocity channel widths.

Each panel in Fig. 7 shows the residual rotation velocity of the galaxy with the corresponding Sérsic index, for different beam sizes. The velocity channel width $\Delta V$ is fixed to $(1/3)V_{diff}$. The beam size varies from 0.5 to 2.0$r_{eqv}$ (as shown by the different colours) for the fixed velocity channel width used in each panel. In each panel, the width of $\Delta V$ and $3\Delta V$ are shown by the dotted and dashed lines, respectively, to show the $1\sigma$ and $3\sigma$ significances of the residual rotation velocity. The error bars have been determined from the standard deviation of the realization of 100 ensemble PVDs.

The residual velocity with 0.5$r_{eqv}$ beam size shown by the blue symbol has a significant difference at the central region in all panels of Fig. 7; the maximum residual is significantly larger than $3\Delta V$. Although the 1.0$r_{eqv}$ beam size (red line) shows a smaller maximum residual than that for the 0.5$r_{eqv}$ beam size, the residual is still significant, being larger than or similar to $3\Delta V$. However, as the beam size increases (i.e. $>2r_{eqv}$), the maximum residual decreases and the significance of the residual rotation velocity does not strongly indicate a rotation velocity due to the SMBH.

For each panel in Fig. 8, different velocity channel widths have been used to generate the PVD of the same galaxy for a fixed 1.0$r_{eqv}$ beam size. Like in Fig. 7, the error bars have been determined from the standard deviation of the realization of 100 ensemble PVDs. The residual velocities for each panel are scaled by the velocity channel width being used. The velocity channel width $\Delta V$ has been adjusted with respect to the required velocity channel width for each panel [$\Delta V_0 = (1/3)V_{diff}$]. Like Fig. 7, as the velocity channel width increases from 0.5 to 2.0$\Delta V_0$, the residual velocity becomes less significant. We find that the choice of $\Delta V \approx 1.0\Delta V_0$ shows a significant ($>3\sigma$) velocity difference for most types of galaxies that we simulated in this work.

In summary, regarding the effect of the spatial resolution, if the radio interferometry beam size is smaller than or similar to $r_{eqv}$, the PVD is clearly resolved and the excess of the rotation velocity due to the SMBH is detected above the $3\sigma$ level when the velocity channel width resolves $(1/3)V_{diff}$. For the effect of the velocity resolution, if the velocity channel width is smaller than $(1/3)V_{diff}$, the effect of the SMBH is detected above the $3\sigma$ level if the scale of $r_{eqv}$ is resolved by the interferometry beam.

## 3.4 Systematic effects

In the previous section, we discussed the spatial and velocity resolution for the PVD analysis using the rotation velocity of pure circular motion without a systematic effect and confirmed our argument that $r_{eqv}$ and $V_{diff}$ set the required beam size and velocity channel width.
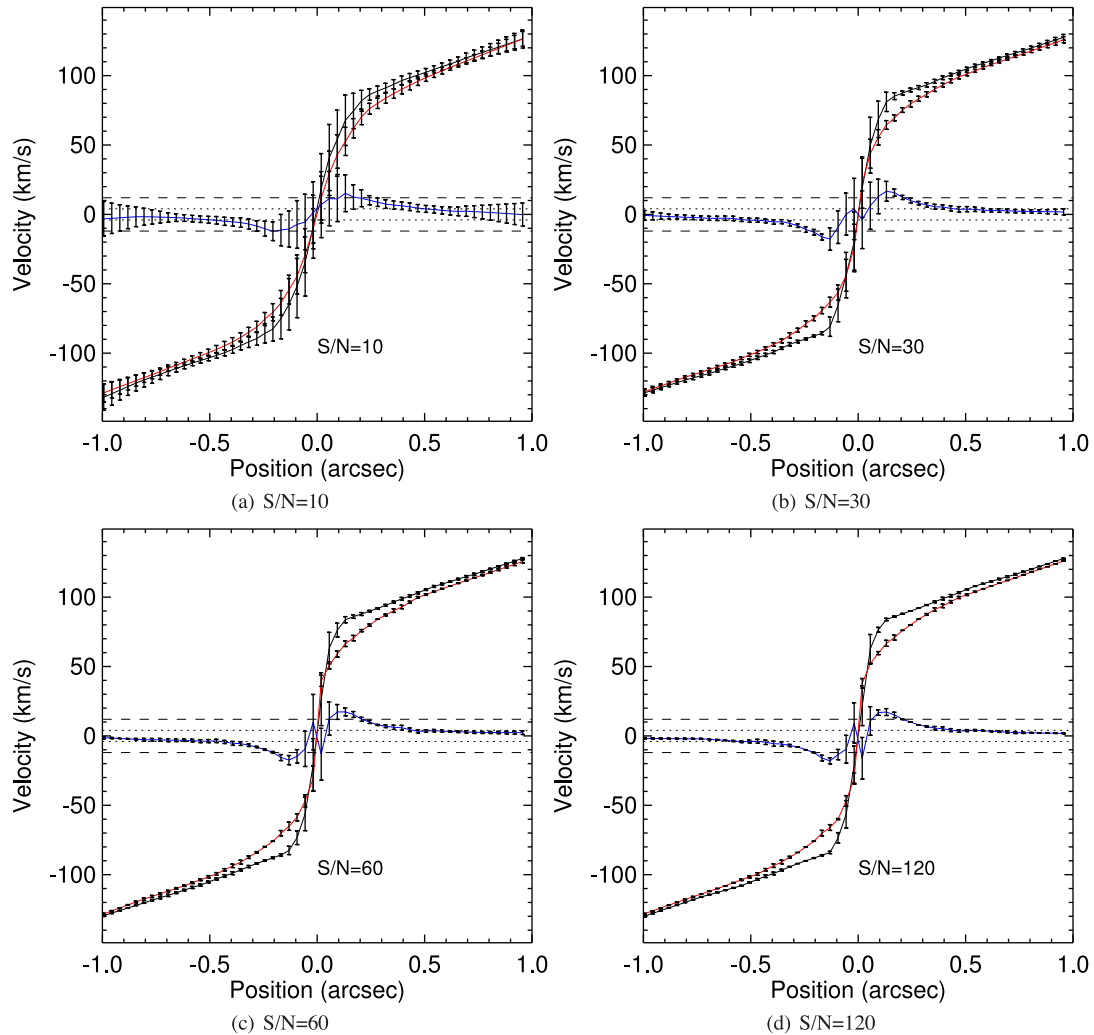
**Figure 6.** Rotation velocities and their residuals of the simulated galaxy with $M_* = 10^{11}$ $M_\odot$ and $M_{BH} = 10^7$ $M_\odot$ measured using 0.15 arcsec beam and 8 km s$^{-1}$ velocity channel width. Each panel shows the same galaxy with a different signal-to-noise ratio: S/N = 10, 30, 60 and 120. The black and red solid lines show the rotation velocity of the galaxy with and without the SMBH and the blue line is the difference between the two rotation velocities. The rotation velocity (solid line) and associated error bar have been determined from the mean and standard deviation of the realization of 100 ensemble PVDs. The velocity uncertainties due to the velocity channel width corresponding to 1 and 3$\sigma$ significances, $(1/3)V_{\text{diff}}$ and $V_{\text{diff}}$, are shown by the dotted and dashed lines.

In this section, we demonstrate the impact of possible systematic effects on the PVD analysis: spatial structure (i.e. gas density distribution) and velocity structure (i.e. inflow/outflow, random motion and warp) as discussed in Section 2.3. We do not perform an extensive search in the parameter space for all these systematic effects and only show the PVD simulations with S/N ≈ 60 for a galaxy with $M_* = 10^{11}$ $M_\odot$ that follows a Sérsic profile with $n = 3$ and hosts a $10^7$ $M_\odot$ SMBH, using the required angular resolution (0.15 arcsec) and velocity channel width (8 km s$^{-1}$). We show the results of simulations using selective parameters for each effect. However, our findings and discussions regarding these systematic effects are valid for the given angular resolution and velocity channel width of the simulated PVD and they can be applied to other galaxies with different $n$ and SMBH masses.

To investigate the systematic effects, we note that one of the disadvantages of using the PVD is that the disc inclination, kinematic position angle and centroid parameters need to be well constrained (Barth et al. 2016). Using more sophisticated methods, including fitting a 3D data cube, may be more reliable and could resolve some

of the issues related with the gas disc geometry. However, we also note that fitting the PVD, on the other hand, has benefited from the better sensitivity to the central velocity upturn and may give better constraints on $M_{BH}$ than fitting a 3D data cube (Barth et al. 2016).

### 3.4.1 Geometry of molecular gas distribution

We consider three different types of density profiles of molecular gas: the same exponential disc profile as the previous simulations but with different scale radius, the same 1 arcsec scale radius exponential disc but with different inclination angles and a density profile with an inner scale radius for density truncation, which mimics the density distribution of a circum-nuclear ring.

First, we perform the test for different gas density profiles by changing the scale radius to adjust the compactness of the profile. Figs 9(a) and (b) show the rotation velocity of the gas disc following the exponential density profile with 0.15 and 0.3 arcsec scale radius and the residual velocity between the rotation velocities of the galaxy with and without a central SMBH. The inclination
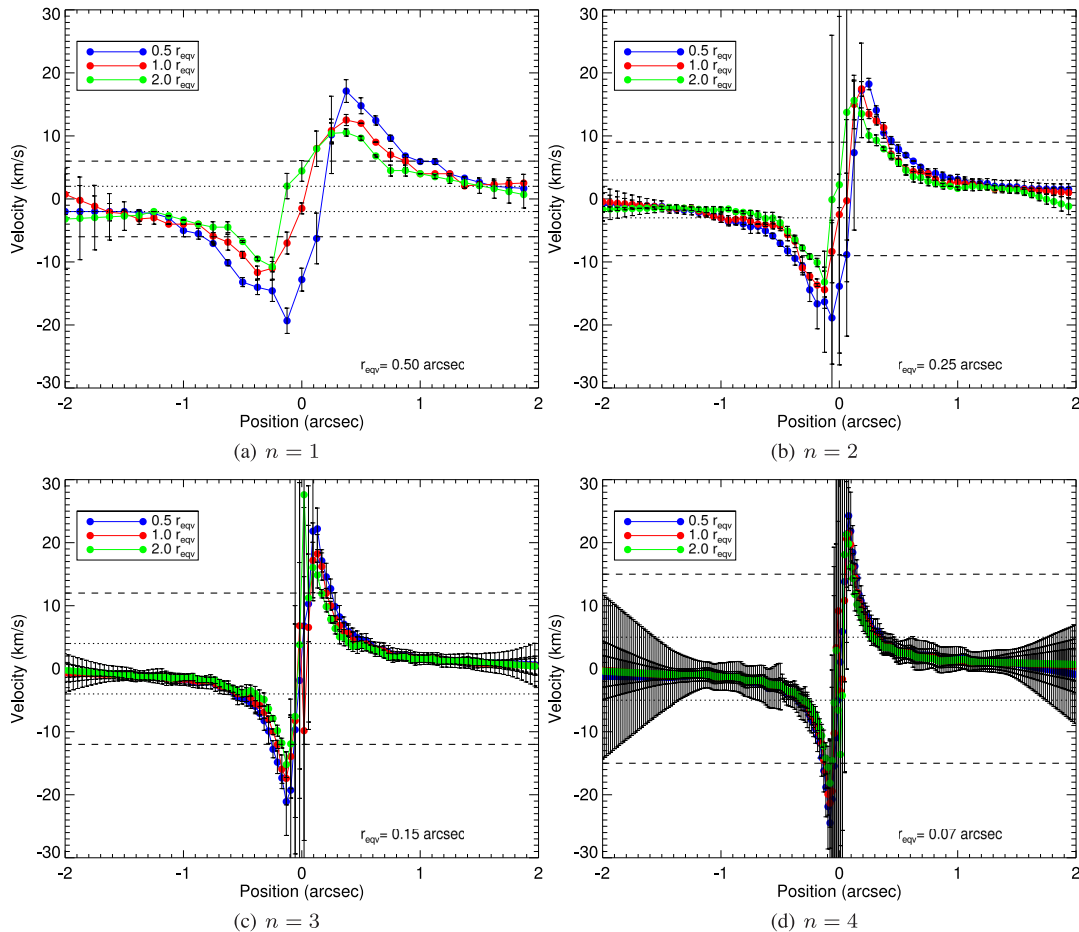
**Figure 7.** Difference between the rotation velocity with and without the SMBH, for the simulated galaxy with $M_* = 10^{11}$ M$_\odot$ and $M_{BH} = 10^7$ M$_\odot$ measured using the same velocity channel width $(1/3)V_{diff}$ but using different beam sizes shown by different colours. Each panel shows the same galaxy with a different Sérsic index from 1 to 4. The error bars have been determined from the standard deviation of the realization of 100 ensemble PVDs. The velocity uncertainties associated with 1 and $3\sigma$ significances, $(1/3)V_{diff}$ and $V_{diff}$, are shown by the dotted and dashed lines.

angle is fixed to $i = 60°$. In this test, the density distribution of the molecular gas is normalized to the integrated density and, therefore, the surface density profile of the molecular gas with a smaller scale radius has a higher peak flux than that with a larger scale radius. Since more signal is concentrated in the central region of the molecular gas disc with 0.15 arcsec scale radius compared with the disc with a 0.3 arcsec radius, the measured velocity for the density profile with a smaller scale radius has smaller error at the central region where the impact of the SMBH is the strongest while it has larger error at the outer region due to the low S/N, as seen in Figs 9(a) and (b), respectively. Comparing the three figures with a similar S/N ($\approx$60) (Fig. 9 a with 0.15 arcsec, Fig. 9 b with 0.30 arcsec and Fig. 6 c with 1.0 arcsec scale radius), we note that the error of the residual velocity at the centre becomes smaller with decreasing scale radius of the molecular gas disc. Also the maximum of the residual velocity is significantly larger than $3\Delta V$ for the gas disc with the smallest scale radius (Fig. 9a). We find that for the same S/N, angular resolution, velocity channel width and inclination angle, a more compact molecular gas density distribution gives a larger significance of the velocity difference in the detection of the SMBH as long as the angular resolution is sufficiently small to resolve $r_{eqv}$.

Secondly, we show the difference of the inclination angle for the same galaxy shown in Fig. 6(c). Figs 9(c) and (d) show the rotation velocity for two different inclination angles, 30° and 80°, instead

of 60° as shown in Fig. 6(c). If the galaxy has small inclination ($i = 30°$), the significance of the velocity difference at the centre between the rotation velocities with and without the SMBH is less than for a large inclination angle because of the velocity projection. The maximum of the residual velocity in Fig. 9(c) is less than $3\sigma$ and lower than that of the higher inclination molecular gas disc shown in Figs 9(d) and 6(c). On the other hand, if the inclination angle becomes even larger and makes the galaxy close to edge on ($i = 80°$) as seen in Fig. 9(d), the synthesized beam includes more molecular gas components with lower velocities migrated from the minor axis and, thus, the overall velocity measurement at the centre is weighted more by the lower velocity components. This issue of the high inclination angle was recently discussed by Barth et al. (2016), who suggested that the projected $r_{SOI}$ along the minor axis has to be resolved to measure the SMBH mass accurately. We remake Fig. 9(d) using a smaller beam $r_{eqv}\cos(i)$ to resolve the projected $r_{eqv}$ along the minor axis, as shown in Fig. 10, which shows that the residual velocity at the central region that was diluted by the lower velocity component as shown in Fig. 9(d) reveals the velocity difference more clearly, although it has large error due to the small beam. We find that for the same S/N, angular resolution, velocity channel width and scale radius of the molecular gas density profile, the significance of the velocity difference increases as the galaxy becomes more inclined; however, for highly inclined galaxies, the
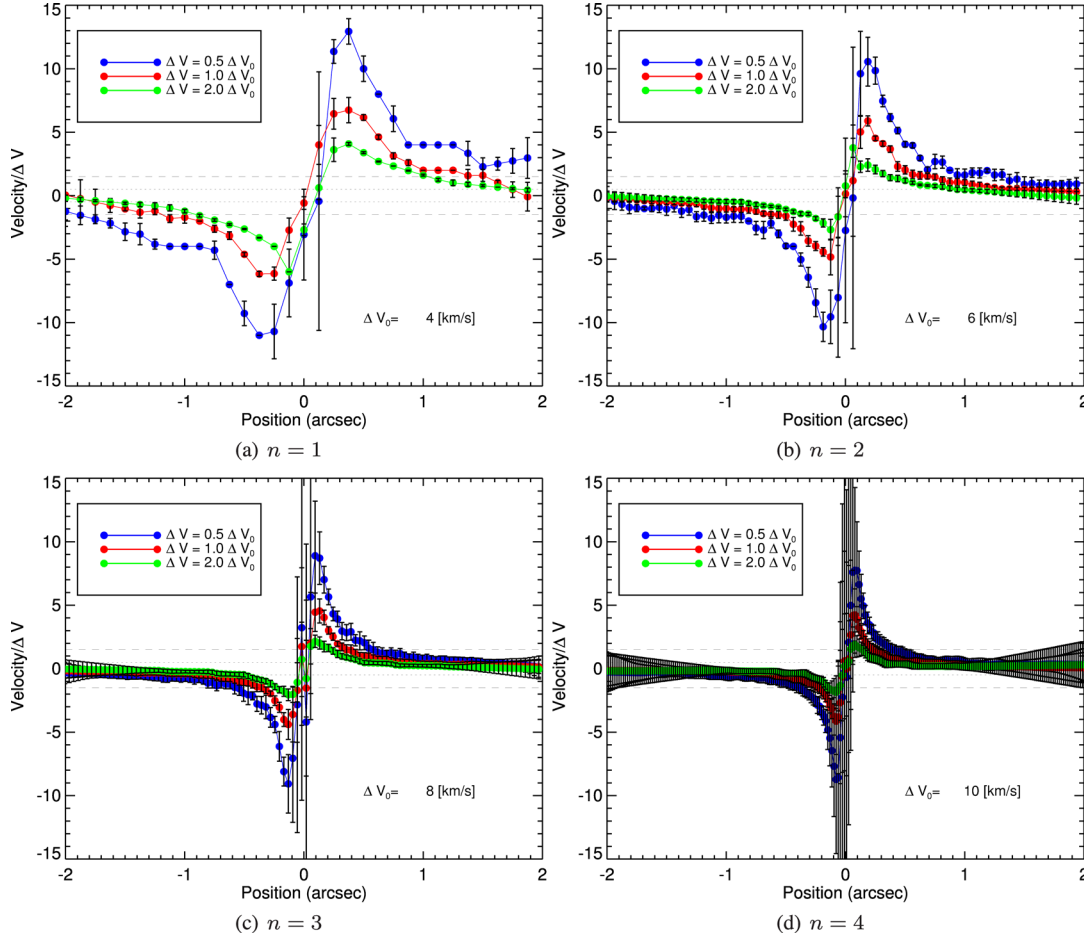
**Figure 8.** Difference between the rotation velocities with and without the SMBH, for the simulated galaxy in Fig. 7 measured using the same beam size $r_{\mathrm{eqv}}$, but using different velocity channel widths as shown by the different colours. Each panel shows the same galaxy with different Sérsic index from 1 to 4. The error bars have been determined from the standard deviation of the realization of 100 ensemble PVDs. The residual velocities for each panel are scaled by the velocity channel width used to generate the PVD for each panel. The uncertainties associated with 1 and 3 times the velocity channel width are shown by the dotted and dashed lines.

beam size should be small enough to resolve a spatial scale with a velocity gradient not much larger than the velocity channel width to avoid the velocity smearing within the beam. Resolving the scale of the projected $r_{\mathrm{eqv}}$ along the minor axis is possible; however, the resulting ALMA beam size ($\approx$0.03 arcsec) will be a practical limitation for observing a galaxy with high inclination. This issue of the high inclination angle can be significantly alleviated by modelling the PVD in position and velocity space together (i.e. a 2D pixel distribution in the PVD) or even completely removed by modelling a 3D data cube, if the S/N of the data is sufficient.

Finally, to test for the circum-nuclear molecular ring, we use the following model density profile, which has often been used to model a proto-planetary disc:

$$\Sigma = \Sigma_0 \left( \frac{r}{R_s} \right)^{-\gamma} \exp \left( \frac{r}{R_s} \right)^{2-\gamma} \sqrt{1 - \frac{R_{\mathrm{in}}}{r}}. \qquad (9)$$

This profile exponentially decreases at $r > R_s$ and has a power-law profile at the centre, like the commonly used profile (e.g. Andrews et al. 2009). However, it has an additional cut-off radius $R_{\mathrm{in}}$ below which the profile truncates very sharply.

Figs 11(a) and (b) show the moment 0 map and PVD for the same galaxy used in this section but for a molecular gas with density profile following equation (9) with $R_s = 1.0$ arcsec and $R_{\mathrm{in}} = 0.15$ arc-

sec. Similarly, Figs 11(c) and (d) show the case with $R_s = 1.0$ arcsec and $R_{\mathrm{in}} = 0.30$ arcsec. As $R_{\mathrm{in}}$ becomes larger, the velocity tracer in the centre disappears and the central region with the strongest impact from the SMBH cannot be probed if the hole size is similar to or larger than $r_{\mathrm{eqv}}$. Figs 11(b) and (d) demonstrate this by showing that for a circum-nuclear gas ring, the significance of the residual velocity at the centre is much smaller than that for the circum-nuclear gas disc if the hole size is similar to or larger than $r_{\mathrm{eqv}}$. For large $R_{\mathrm{in}}$ (0.3 arcsec), the velocity at the centre in Fig. 11(d) was linearly interpolated using the velocity measurements in the outer region.

### 3.4.2 Non-circular velocity structure

We consider three different systematic velocity structures (outflow, random motion and disc warp) and demonstrate how they distort the PVD from pure circular motion.

First, we consider the impact of the outflow velocity in the circum-nuclear molecular gas. The inflow and outflow are included in the velocity field in KINMS using the formalism of KINEMETRY (Krajnović et al. 2006). We note that KINEMETRY only models a smooth inflow and outflow in the plane of the molecular gas disc and more violent molecular gas outflows (which we do not consider in this work) may have distinct position angles from the main body
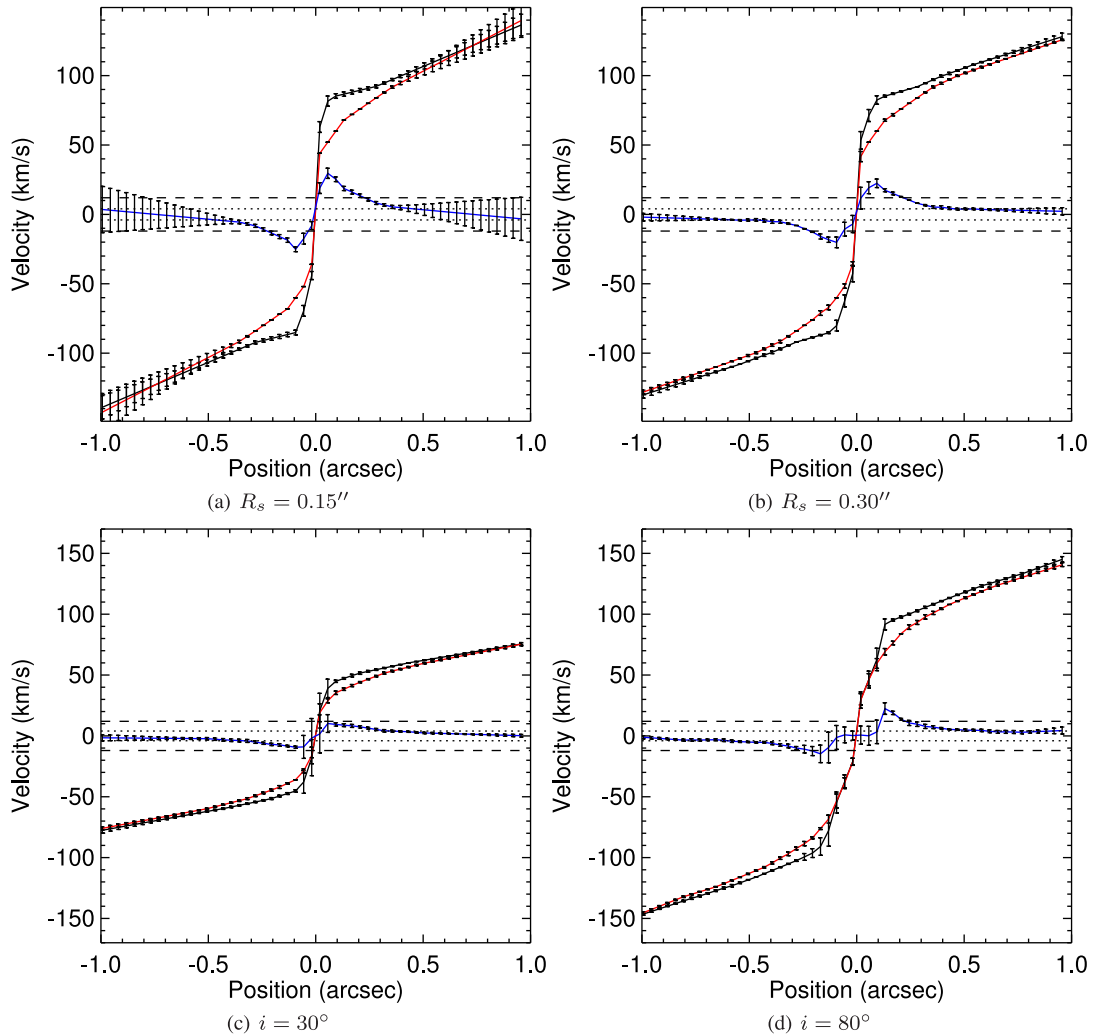
(a) $R_s = 0.15''$



(b) $R_s = 0.30''$



(c) $i = 30°$



(d) $i = 80°$

**Figure 9.** Rotation velocities and their residuals for the simulated galaxy in Fig. 6(c) but using a different scale radius and inclination for the gas disc. The same beam size $r_{eqv}$ (0.15 arcsec) and velocity channel width (8 km s$^{-1}$) are used for all simulations. The error bars have been determined from the standard deviation of the realization of 100 ensemble PVDs. The residual velocity for each panel is scaled by the velocity channel width used to generate the PVD for each panel. The uncertainties associated with 1 and 3 times the velocity channel width are shown by the dotted and dashed lines.
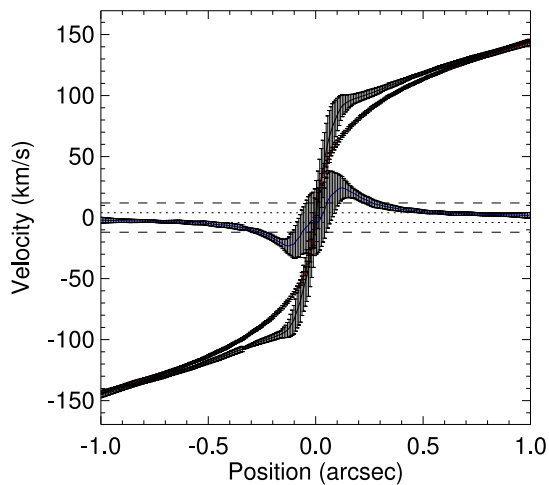


**Figure 10.** Same as Fig. 9(d) but using a higher angular resolution to resolve the projected $r_{eqv}$ along the minor axis, $r_{eqv} \cos(i)$. The beam size is 0.03 arcsec.

of the gas disc. Figs 12(a) and (b) show the rotation velocities of the galaxy with and without the SMBH and the difference of the two velocities for the same galaxy used in Fig. 6(c), which, however, has small (20 km s$^{-1}$) and large (60 km s$^{-1}$) constant radial outflow velocity in the input velocity profile. $V_{diff}$ for this galaxy is 24 km s$^{-1}$. If the outflow velocity is small compared with $V_{diff}$, as seen in Fig. 12(a), the velocity structure is still dominated by the circular motion and the residual velocity shows a $>3\sigma$ deviation at angular scale $r_{eqv}$. However, if the outflow velocity is significantly larger than $V_{diff}$, as seen in Fig. 12(b), the error bar of the residual velocity in the central region is larger than $3\sigma$ deviation and the signature of the maximum deviation seen in Fig. 12(a) is not significant any more.

Secondly, we consider the impact of a random velocity dispersion in the molecular gas. Figs 12(c) and (d) show the rotation velocities of the galaxy with and without a SMBH and the difference of the two velocities for the same galaxy used in Fig. 6(c), which, however, has a small (4 km s$^{-1}$) and large (16 km s$^{-1}$) random velocity dispersion in the input velocity profile, compared with the 8 km s$^{-1}$ velocity channel width used in Fig. 6(c). If the random velocity dispersion is smaller than the velocity channel width (Fig. 12c), the velocity
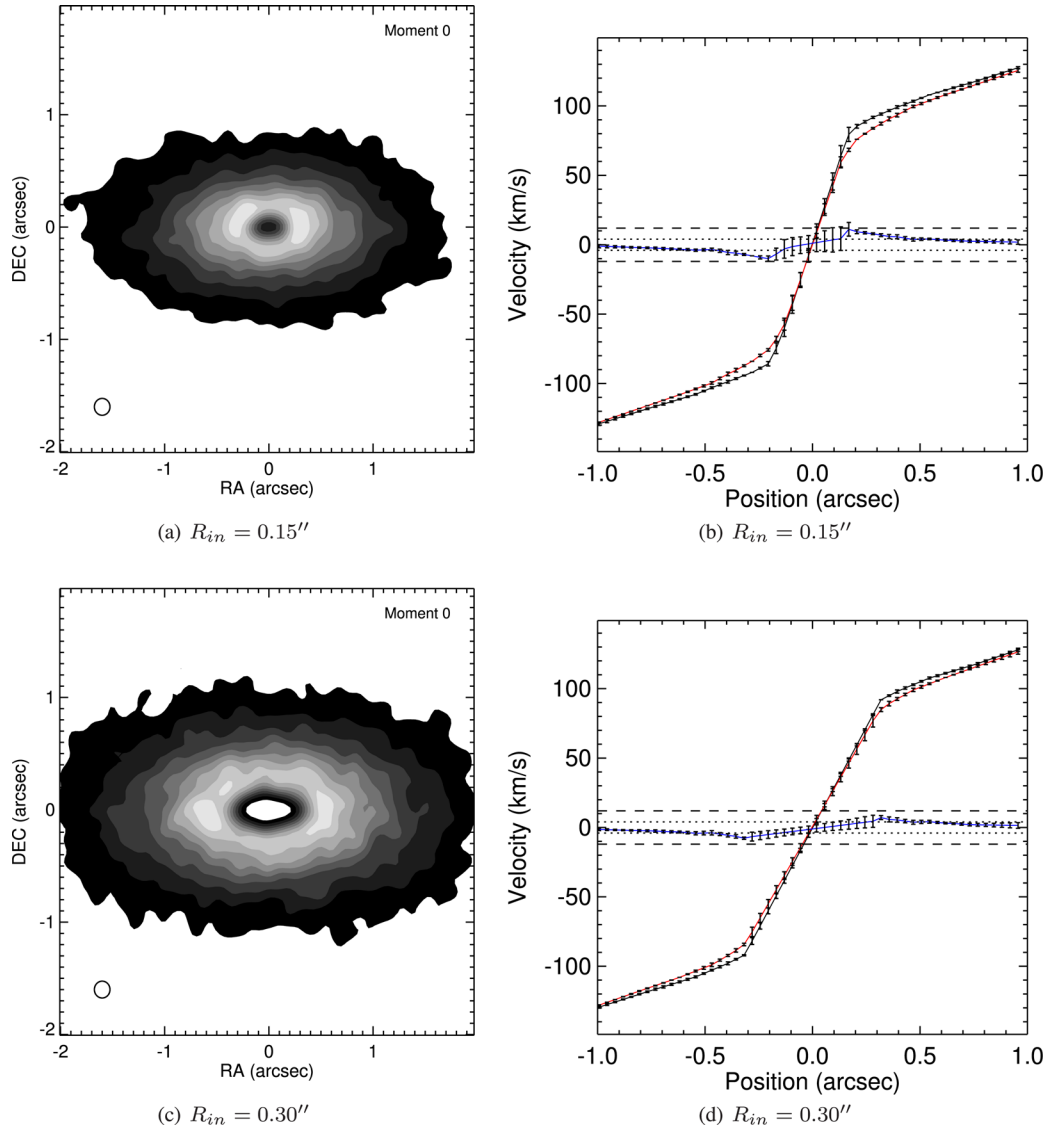
(a) $R_{in} = 0.15''$



(b) $R_{in} = 0.15''$



(c) $R_{in} = 0.30''$



(d) $R_{in} = 0.30''$

**Figure 11.** Moment 0 map (right-hand panels) and rotation and residual velocity (left-hand panels) of the simulated galaxy in Fig. 6(c) measured using the required beam size $r_{eqv}$ (0.15 arcsec) and velocity channel width (8 km s$^{-1}$), but using a gas density distribution with an inner hole. For fixed $R_s = 1$ arcsec in equation (9), $R_{in} = 0.15$ and 0.30 arcsec were used for the upper and lower panels, respectively. $R_{in} = 0.15$ arcsec is the same as the beam size required to detect the SMBH for this galaxy. The error bars have been determined from the standard deviation of the realization of 100 ensemble PVDs. The residual velocities are scaled by the velocity channel width used to generate the PVD for each panel. The uncertainties associated with 1 and 3 times the velocity channel width are shown by the dotted and dashed lines. Note that if there is no velocity measurement in the centre, the velocity measurement is linearly interpolated to the centre.

broadening in the PVD is mild and the significance of the residual velocity is not much contaminated by errors. However, if the random velocity is larger than the channel width (Fig. 12d), the residual velocity shows a larger error and there is a decreasing significance of the velocity difference due to the SMBH. Therefore, to detect the SMBH for a given spatial resolution and galaxy mass profile, care should be taken in the choice of the velocity channel width, which should be significantly smaller than the random velocity dispersion in the molecular gas, which is, however, difficult to know a priori and needs to be included in the modelling if necessary.

Last, we consider a warped disc of molecular gas. If the warped disc is projected on to the sky, the position angle of the disc gradually varies from the centre to the outer region. As a result, the warped disc introduces an uncertainty in the determination of the kinematic major axis from the PVD. Fig. 13(a) shows the velocity field (or

moment 1 map) of the warped disc simulated by changing the position angle from 240° to 270° as a function of the radius. The major axis is determined by the position angle at the outer region (i.e. $i = 270°$) and the innermost region has a 30° offset. Like the other tests, every other parameter is the same as the ones in Fig. 6(c). Unlike the regular symmetric spider diagram due to pure rotation, the velocity field of the warped disc shows a distortion at the centre. Because of the incorrect major axis in the PVD analysis, the rotation velocity in the region where the warping is occurring can be underestimated depending on the velocity measurement methods (Sofue & Rubin 2001). Fig. 13(b) shows the rotation velocities of the galaxy with and without the SMBH and the difference between the two velocities. Although the envelope-tracing method used for our tests traces the terminal velocity, which was not much affected by warping as shown by comparison with Fig. 6(c), more sophisticated
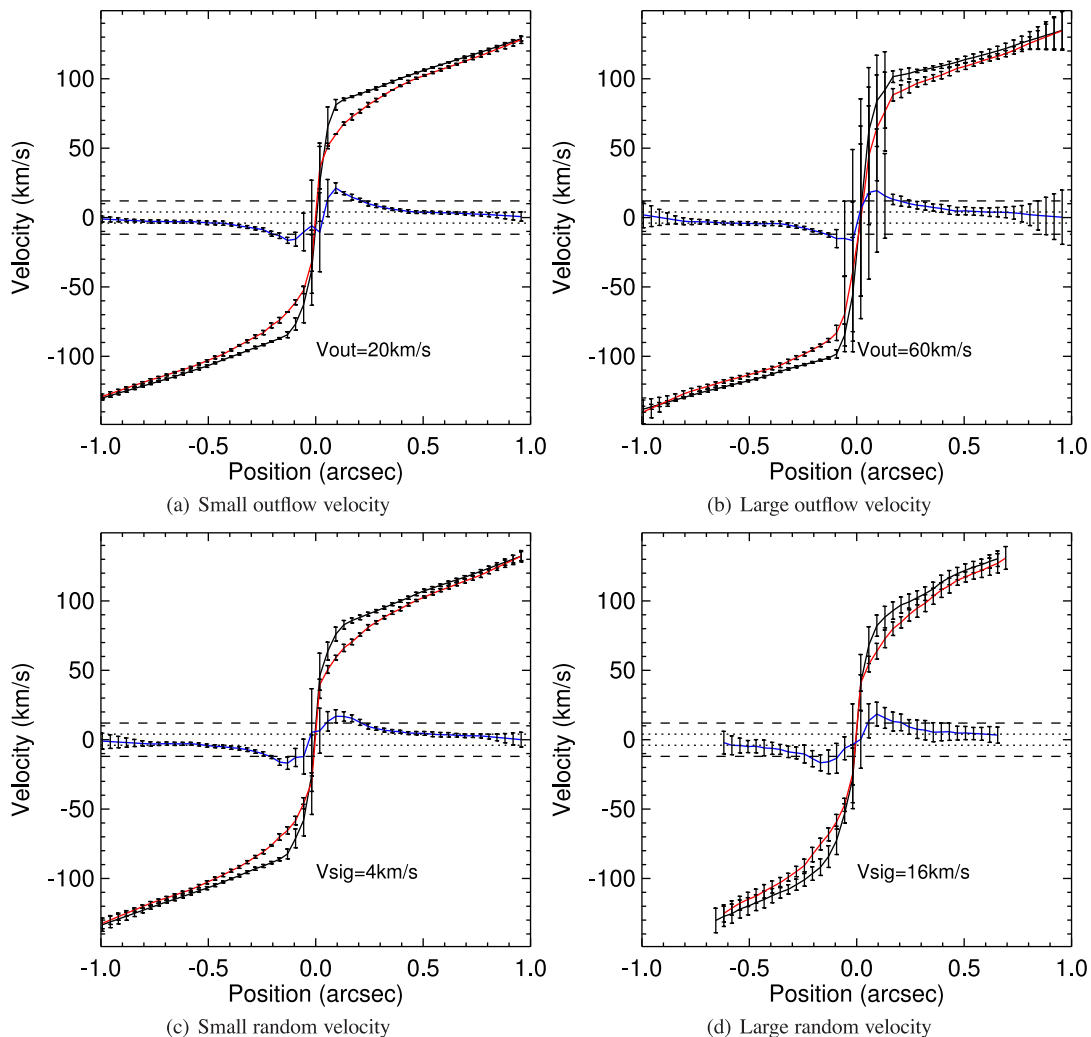
**Figure 12.** Rotation velocities and their residuals for the simulated galaxy in Fig. 6(c) measured using the required beam size $r_{eqv}$ (0.15 arcsec) and velocity channel width (8 km s$^{-1}$), but using different outflow and random velocities for the gas disc. The error bars have been determined from the standard deviation of the realization of 100 ensemble PVDs. The residual velocities for each panel are scaled by the velocity channel width used to generate the PVD for each panel. The uncertainties associated with 1 and 3 times the velocity channel width are shown by the dotted and dashed lines.

methods (e.g. Józsa et al. 2007) are required for detailed modelling of the warped disc to infer the SMBH mass.

### 3.5 Surface brightness profile bias

In Section 2.4, we show that the systematic error of the galaxy surface brightness profile due to the poor resolution of a galaxy image may bias the inference of the SMBH mass, as illustrated in Fig. 4. We simulate two galaxy PVDs using the same rotation velocities of the core-Sérsic profiles in Fig. 4. However, in this demonstration, we shift the rotation velocities in Fig. 4 along the *x*-axis by moving the galaxy closer and we simulate the PVD using a 0.15 arcsec beam size instead of the 0.01 arcsec beam size shown in Fig. 4, by assuming that the galaxy photometric image does not resolve the galaxy core profile and that the ALMA beam also cannot resolve the difference between the true rotation velocity and the biased velocity due to the galaxy surface brightness profile bias. We simulate the PVD using the same 0.15 arcsec beam size and 8 km s$^{-1}$ velocity channel width for two core-Sérsic galaxies, one with $\gamma = 0.1$ (Fig. 14a) and the other with $\gamma = 0.5$ (Fig. 14b).

Then we measure the SMBH masses in these galaxies by modelling their rotation velocities to demonstrate the effect of bias in the measurement of the galaxy surface brightness profile. Thus, we assume that the galaxy surface brightness profile is accurately determined beyond the radius larger than the seeing of an optical or near-infrared image and fix the Sérsic index parameter to the true value, since the cores of these galaxies are assumed not to be resolved. This is the biased galaxy surface brightness profile used for the demonstration. The two free parameters are the SMBH mass and the mass-to-light ratio. On a 2D grid space of the SMBH mass and mass-to-light ratio, we compute a $\chi^2$ per degree of freedom by comparing the true rotation velocity and the model rotation velocity generated from the biased galaxy surface brightness profile with varying mass-to-light ratio and SMBH mass. We assume a constant error of the data point, which is related only to the velocity channel width, $\sigma_v = \sqrt{0.5}\Delta V$ (Davis 2014). In addition to the channel width, the real error also includes the uncertainty of the velocity measurement using the galaxy surface brightness profile. However, we neglect this uncertainty since we assume that the galaxy surface brightness profile is accurately determined down to the scale of
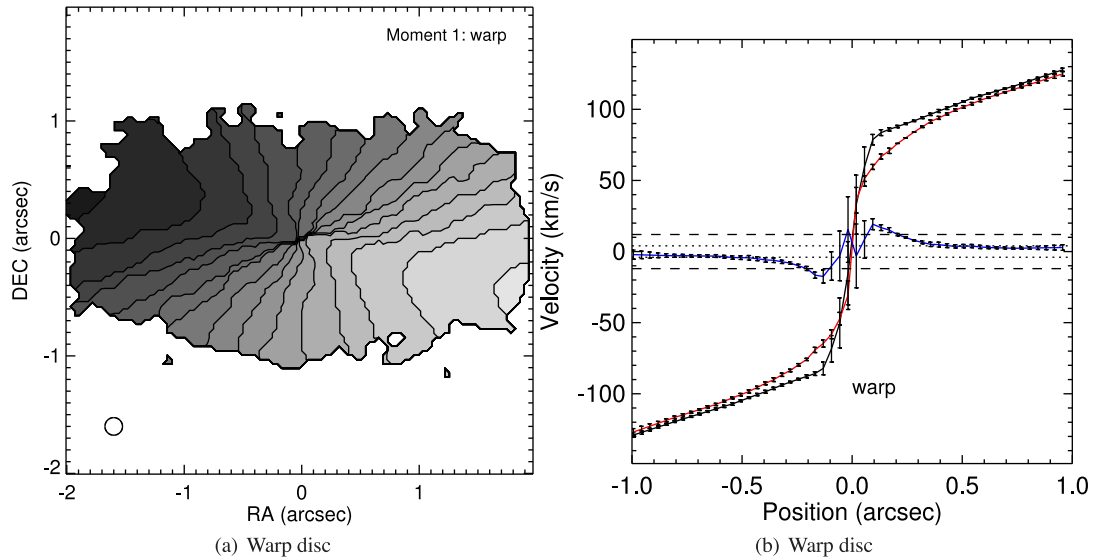
(a) Warp disc                                    (b) Warp disc

**Figure 13.** Velocity field (left-hand panel) and rotation and residual velocity (right-hand panel) of the simulated galaxy in Fig. 6(c) measured using the required beam size $r_{eqv}$ (0.15 arcsec) and velocity channel width (8 km s$^{-1}$), but using the velocity structure for a warped gas disc. If projected, the warped disc appears with varying position angle. The difference between the position angles at the innermost and the outermost regions is 30$^{\circ}$. The error bars have been determined from the standard deviation of the realization of 100 ensemble PVDs. The residual velocities for each panel are scaled by the velocity channel width used to generate the PVD for each panel. The uncertainties associated with 1 and 3 times the velocity channel width are shown by the dotted and dashed lines.
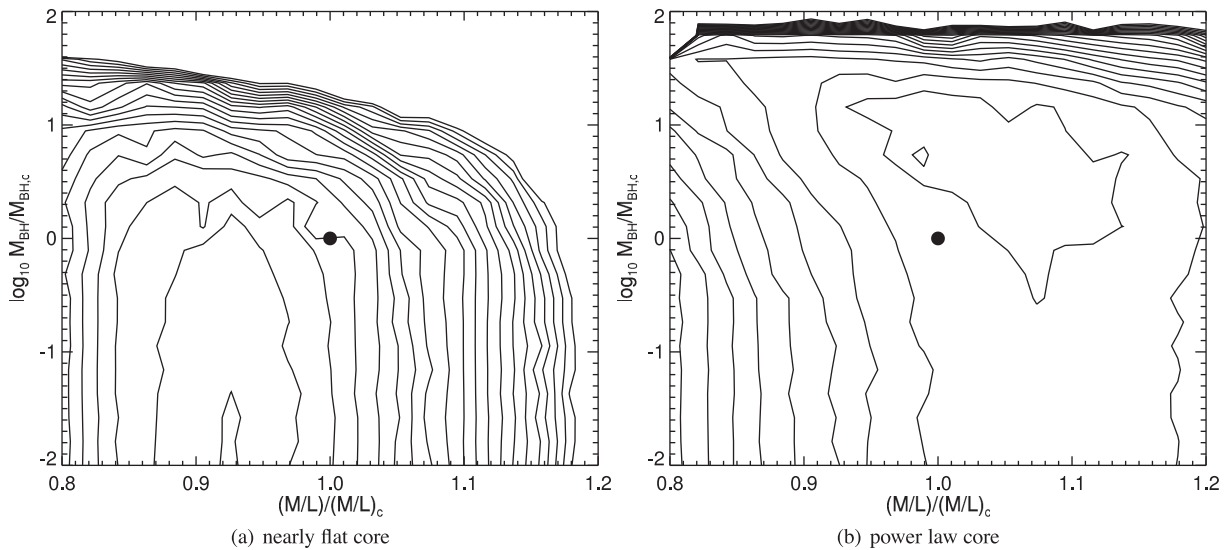


(a) nearly flat core                              (b) power law core

**Figure 14.** Contour of $\chi^2$ per degree of freedom of the model rotation velocity for the core-Sérsic galaxy with the nearly flat core seen in Fig. 4(a) and the power-law core seen in Fig. 4(b). The galaxy surface brightness is assumed to be accurately determined without bias for a radius larger than the seeing of the galaxy image. The two free parameters (SMBH mass and mass-to-light ratio) are normalized by the true value used for simulating each galaxy. The black point in the middle of each panel indicates the location of the true parameter. The largest probability in $\chi^2$ is offset from the location of the true parameter, biasing the SMBH mass by an order of magnitude with a small change of the mass-to-light ratio.

image seeing and only the mass-to-light ratio changes the galaxy rotation velocity.

Figs 14(a) and (b), respectively, show the contour of $\chi^2$ per degree freedom of the model rotation velocity for the simulated core-Sérsic galaxy in Figs 4(a) and (b). The two free parameters (SMBH mass and mass-to-light ratio) are normalized by the true SMBH and mass-to-light ratio. The black point in the middle of each figure indicates the location of the true parameter. For the galaxy with the nearly flat core shown in Fig. 14(a), the best $\chi^2$ value region is systematically offset from the location of the true parameter such that the SMBH mass is >10 times smaller and the mass-to-light ratio is ≈5 per cent

smaller than the true value. For the galaxy with the power-law core shown in Fig. 14(b), the best $\chi^2$ region is also offset from the true parameter such that the SMBH mass is ≈10 times larger and the mass-to-light ratio is ≈3 per cent smaller than the true value.

Figs 14(a) and (b) demonstrate that if the galaxy core profile in the photometric image is not resolved and the determination of the stellar mass distribution in the centre is slightly biased, the SMBH mass can be biased by more than an order of magnitude, though this is compensated for by a small change in the mass-to-light ratio. This systematic bias in the SMBH mass is much larger than the fitting error (20–80 per cent, e.g. Davis et al. 2013a; Onishi
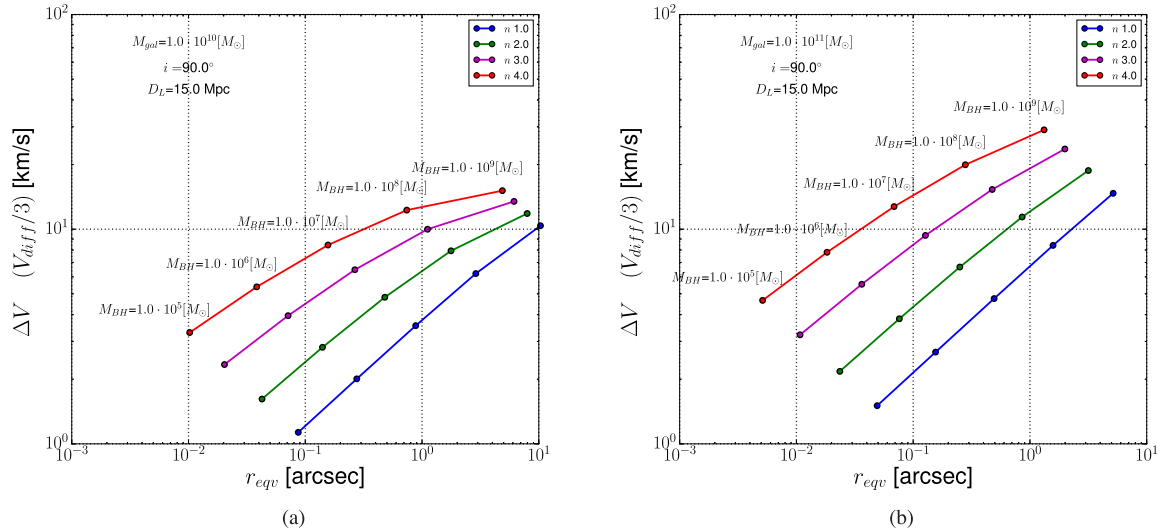
**Figure 15.** Parameter space of the required beam size and velocity channel width for detecting the SMBH mass, which is shown by the circle with appropriate annotation. A fiducial galaxy with $M_* = 10^{10}$ M$_\odot$ (left) and $M_* = 10^{11}$ M$_\odot$ (right) with inclination $i = 90$ is assumed to be at 15 Mpc distance. Colours indicate galaxy surface brightness profiles determined by Sérsic index ($n = 1, 2, 3, 4$). Using the relevant galaxy inclination and distance, one can shift the points and estimate the required beam size and velocity channel width to detect the SMBH mass that one aims to detect.

et al. 2015) and can be even larger depending on the galaxy profile shape and the angular resolution of the galaxy image. This confirms our argument in Section 2.4 and implies that the spatial resolution of the galaxy image and the beam size of the radio interferometry should be similar and both have to be comparable to the $r_{\rm eqv}$ of the target galaxy to obtain an accurate SMBH mass without large bias.

## 4 DISCUSSION

Since only a few SMBH mass measurements using molecular gas kinematics with high-resolution radio interferometry have been reported (e.g. Davis et al. 2013a; Onishi et al. 2015; Barth et al. 2016) at the time of writing, it is difficult to validate our arguments using real observations. Nevertheless, Davis (2014) analyses the molecular gas kinematics of NGC 4526 using different beam sizes to demonstrate that reliable inference of SMBH mass is possible with a beam size larger than $r_{\rm SOI}$. The beam size (i.e. 0.25 arcsec) used in the original paper reporting the mass of the SMBH in NGC 4526 (Davis et al. 2013a) is close to the SMBH $r_{\rm SOI}$ inferred by the $M$–$\sigma$ relation (Gültekin et al. 2009) and a consistent measurement of the SMBH mass has been obtained using up to a 1 arcsec beam (Davis 2014), which is 4 times larger than $r_{\rm SOI}$. Interestingly, we note that $r_{\rm eqv}$ for NGC 4526 also corresponds to 1 arcsec based on the assumed SMBH mass ($2 \times 10^8$ M$_\odot$) and the luminosity distance (16.4 Mpc) used in Davis et al. (2013a), if we adopt the known Sérsic index ($n = 2.7$, Krajnović 2013) and the galaxy stellar mass ($M_* = 10^{11}$ M$_\odot$, Capetti et al. 2009) from the literature. This suggests that $r_{\rm eqv}$ as the minimum spatial resolution required for a SMBH mass measurement also makes sense for the real observational data.

Based on the simple discussions of the galaxy rotation velocity and the analysis of simulated PVDs, we argue that for a given galaxy stellar mass ($M_*$), surface brightness profile shape ($n$), inclination ($i$) and luminosity distance ($D_{\rm L}$), there is a minimum requirement of the spatial and velocity resolution to resolve the PVD to detect the SMBH mass that one aims to detect, which will be an upper limit if not detected. This allows us to investigate the capability of ALMA

in the parameter space of the beam size and velocity channel width, for the given galaxy observational parameters ($M_*$, $n$, $i$ and $D_{\rm L}$).

In Fig. 15, we show the locations of $M_{\rm BH}$ in the parameter space of the required beam size and velocity channel width to resolve the PVD to detect the SMBH. Figs 15(a) and (b) show a galaxy with $M_* = 10^{10}$ M$_\odot$ and $M_* = 10^{11}$ M$_\odot$, respectively. Different colours indicate galaxy Sérsic indices and each round symbol indicates the location of the SMBH mass as annotated. We set the luminosity distance $D_{\rm L} = 15$ Mpc ($z = 0.0035$ for the adopted cosmology in this study) and $i = 90°$ in Fig. 15. If needed, the value of $\Delta V$ can be adjusted by multiplying by $\sin(i)$ for a given galaxy inclination and the value of $r_{\rm eqv}$ can be adjusted by multiplying by the ratio between the angular diameter distance at $D_{\rm L} = 15$ Mpc and at $D_{\rm L}$ where the galaxy is actually located, using the available red shift. However, we emphasize that $\Delta V$ and $r_{\rm eqv}$ are, in practice, limited by the systematic velocity structure and angular resolution of the photometric image, as we discussed in previous sections.

As the SMBH mass that one aims to detect decreases, both $\Delta V$ and $r_{\rm eqv}$ also decrease for all types of galaxies. In more detail, for a galaxy with lower Sérsic index, the required angular and velocity resolution is routinely achievable by ALMA. For example, Fig. 15(b) implies that a small SMBH with mass as low as $10^5$ M$_\odot$ within a galaxy with $M_* = 10^{11}$ M$_\odot$ and $i = 60°$ whose surface brightness profile follows the Sérsic model with $n = 3$ can be detected at a distance up to the Virgo cluster (15 Mpc) using a 0.01 arcsec beam size and 2.5 km s$^{-1}$ velocity channel width based on the assumption that the galaxy surface brightness profile is determined without large bias and the velocity uncertainty in the circum-nuclear molecular gas is properly modelled with small residual error ($<2.5$ km s$^{-1}$). For fixed SMBH mass, $r_{\rm eqv}$ becomes larger and $\Delta V$ becomes smaller, as the galaxy surface brightness profile becomes less concentrated. The effect is more prominent for the spatial resolution, and therefore, the disadvantage of decreasing $\Delta V$ (increasing velocity resolution) is better compensated for by the advantage of increasing the beam size. For late-type galaxies, one can take advantage of this large $r_{\rm eqv}$ to reach the lower SMBH mass by increasing the velocity resolution. A high velocity resolution increases the data volume but is easily achievable by ALMA,

unlike the spatial resolution, which is limited by the physical array configuration.

Based on the results in this work, we argue that for a typical 1D velocity dispersion (e.g. 7 km s$^{-1}$ in Mogotsi et al. 2016) of molecular gas in nearby galaxies, ALMA can detect a SMBH mass larger than $10^7$ M$_\odot$ for nearly all types of galaxies with $M_* = 10^{11}$ M$_\odot$ for $n > 2$ within 15 Mpc distance, using high angular resolution (0.05 arcsec) and velocity channel width ($\Delta V = 7$ km s$^{-1}$). If we use a larger $\Delta V \approx 10$ km s$^{-1}$, the minimum detectable black hole mass is $\approx 10^6$ M$_\odot$ for $n = 4$ Sérsic profile galaxies. This is consistent with fig. 7 in Davis (2014).

In principle, the same exercise can be done when proposing ALMA observations to measure the gas kinematics to detect a SMBH. Although a real galaxy surface brightness profile does not follow the Sérsic model, this exercise provides a rough estimate of the angular resolution and velocity channel width for ALMA to detect the SMBH with an expected mass, for a wide range of galaxy morphology types. This study will serve as a simple but useful technical justification for the ALMA proposal with the science goal of measuring SMBH mass using molecular gas kinematics.

## 5 SUMMARY

By generalizing and extending the work of Davis (2014), we studied the potential merits of the technique using molecular gas kinematics to measure SMBH mass. We combined an analytic argument and realistic PVD simulations by considering the relevant spatial and velocity resolutions, the systematic effect in the spatial and velocity structure of the circum-nuclear molecular gas and the impact of a biased galaxy surface brightness profile shape. The simple analytic argument suggests that the effect of the SMBH can be detected at a spatial scale where the rotation velocities due to the SMBH and the galaxy stellar mass distribution become equal $r_{eqv}$, which is larger than $r_{SOI}$ by a factor of a few for early-type galaxies and by an order of magnitude for late-type galaxies. We find that the increased $r_{eqv}$ for less concentrated galaxies is an advantage for measuring the SMBH mass in late-type galaxies. The velocity channel width also has to be $(1/3)V_{diff}$ to resolve the velocity difference with a $3\sigma$ significance level.

However, systematic effects due to the spatial and velocity structure in the circum-nuclear molecular gas affect the rotation velocity measurement. We find that the signature of the SMBH is more clearly detected: (1) if the molecular gas surface density profile is more compact, (2) if the gas disc is inclined as much as possible but the projected $r_{eqv}$ along the minor axis is still resolved by the observing beam size and (3) if there are enough gas clouds in the centre to trace the kinematics. We also find that the systematic motion of the molecular gas affects the galaxy PVD. Therefore, if it exists, the gas outflow should be smaller than $V_{diff}$ and the random velocity dispersion should be smaller than the velocity channel width. Disc warp, if it exists, introduces an uncertainty in the kinematic major axis and may distort the kinematics along the major axis, which needs to be considered in the rotation velocity measurement. In addition, we illustrate the impact of the systematic error introduced by an incorrect measurement of the galaxy surface brightness profile due to the insufficient resolution of a galaxy image when resolving the core surface brightness profile. Depending on the shape of galaxy surface brightness profile and the resolution of the galaxy photometric image, the SMBH mass can be largely biased and this systematic error can be larger than the fitting error. Therefore, both the resolution of the photometric image and the radio interferometry

beam have to be small enough to resolve $r_{eqv}$ for a given galaxy to minimize the bias.

We use the IDL program KINMS (Davis et al. 2013b) to simulate the observed PVDs of galaxies with a SMBH including observational measurement processes with noise and systematic effects. The analysis of the measured rotation velocity from a simulated PVD demonstrates the validity of our arguments and confirms our intuitions for the impact of the SMBH on the rotation velocity of the circum-nuclear molecular gas disc. This work provides useful guidance in the analysis of a galaxy PVD for SMBH mass measurement and a technical justification for the ALMA proposal to observe the kinematics of molecular gas in galactic centres to measure the SMBH mass.

## REFERENCES

Andrews S. M., Wilner D. J., Hughes A. M., Qi C., Dullemond C. P., 2009, ApJ, 700, 1502
Araya Salvo C., Mathur S., Ghosh H., Fiore F., Ferrarese L., 2012, ApJ, 757, 179
Barth A. J., Sarzi M., Rix H.-W., Ho L. C., Filippenko A. V., Sargent W. L. W., 2001, ApJ, 555, 685
Barth A. J., Darling J., Baker A. J., Boizelle B. D., Buote D. A., Ho L. C., Walsh J. L., 2016, ApJ, 823, 51
Bower G. A. et al., 2001, ApJ, 550, 75
Caon N., Capaccioli M., D'Onofrio M., 1993, MNRAS, 265, 1013
Capetti A., Kharb P., Axon D. J., Merritt D., Baldi R. D., 2009, AJ, 138, 1990
Ciotti L., Bertin G., 1999, A&A, 352, 447
Combes F. et al., 2014, A&A, 565, A97
Davis T. A., 2014, MNRAS, 443, 911
Davis T. A., Bureau M., Cappellari M., Sarzi M., Blitz L., 2013a, Nature, 494, 328
Davis T. A. et al., 2013b, MNRAS, 429, 534
den Brok M. et al., 2015, ApJ, 809, 101
Emsellem E., Monnet G., Bacon R., 1994, A&A, 285, 723
Ferrarese L., Ford H., 2005, Space Sci. Rev., 116, 523
Ferrarese L., Merritt D., 2000, ApJ, 539, L9
Ferrarese L., Ford H. C., Jaffe W., 1996, ApJ, 470, 444
Filippenko A. V., Ho L. C., 2003, ApJ, 588, L13
García-Burillo S. et al., 2014, A&A, 567, A125
García-Ruiz I., Sancisi R., Kuijken K., 2002, A&A, 394, 769
Gebhardt K. et al., 2000, ApJ, 539, L13
Graham A. W., 2001, AJ, 121, 820
Graham A. W., Erwin P., Trujillo I., Asensio Ramos A., 2003, AJ, 125, 2951
Gültekin K. et al., 2009, ApJ, 698, 198
Häring N., Rix H.-W., 2004, ApJ, 604, L89
Izumi T. et al., 2013, PASJ, 65, 100
Józsa G. I. G., Kenn F., Klein U., Oosterloo T. A., 2007, A&A, 468, 731
Kormendy J., 1988, ApJ, 325, 128
Kormendy J., Ho L. C., 2013, ARA&A, 51, 511
Krajnović D., 2013, MNRAS, 432, 1768
Krajnović D., Cappellari M., de Zeeuw P. T., Copin Y., 2006, MNRAS, 366, 787
Magorrian J. et al., 1998, AJ, 115, 2285
Marconi A., Hunt L. K., 2003, ApJ, 589, L21

Mateos S., Alonso-Herrero A., Carrera F. J., Blain A., Severgnini P., Caccianiga A., Ruiz A., 2013, MNRAS, 434, 941

McAlpine W., Satyapal S., Gliozzi M., Cheung C. C., Sambruna R. M., Eracleous M., 2011, ApJ, 728, 25

McConnell N. J., Ma C.-P., 2013, ApJ, 764, 184

McConnell N. J., Ma C.-P., Gebhardt K., Wright S. A., Murphy J. D., Lauer T. R., Graham J. R., Richstone D. O., 2011, Nature, 480, 215

Miyoshi M., Moran J., Herrnstein J., Greenhill L., Nakai N., Diamond P., Inoue M., 1995, Nature, 373, 127

Mogotsi K. M., de Blok W. J. G., Caldú-Primo A., Walter F., Ianjamasi-manana R., Leroy A. K., 2016, AJ, 151, 15

Onishi K., Iguchi S., Sheth K., Kohno K., 2015, ApJ, 806, 39

Reines A. E., Sivakoff G. R., Johnson K. E., Brogan C. L., 2011, Nature, 470, 66

Richstone D. et al., 1998, Nature, 395, A14

Sarzi M., Rix H.-W., Shields J. C., Rudnick G., Ho L. C., McIntosh D. H., Filippenko A. V., Sargent W. L. W., 2001, ApJ, 550, 65

Satyapal S., Secrest N. J., McAlpine W., Ellison S. L., Fischer J., Rosenberg J. L., 2014, ApJ, 784, 113

Sersic J. L., 1968, Atlas de galaxias australes. Observatorio Astronomico. Cordoba, Argentina

Seth A. C. et al., 2010, ApJ, 714, 713

Shankar F. et al., 2016, MNRAS, 460, 3119

Shen S., Mo H. J., White S. D. M., Blanton M. R., Kauffmann G., Voges W., Brinkmann J., Csabai I., 2003, MNRAS, 343, 978

Silk J., Mamon G. A., 2012, Res. Astron. Astrophys., 12, 917

Sofue Y., Rubin V., 2001, ARA&A, 39, 137

Stern D. et al., 2012, ApJ, 753, 30

Tremaine S. et al., 2002, ApJ, 574, 740

Trujillo I., Erwin P., Asensio Ramos A., Graham A. W., 2004, AJ, 127, 1917

van den Bosch R. C. E., Gebhardt K., Gültekin K., van de Ven G., van der Wel A., Walsh J. L., 2012, Nature, 491, 729

Vergani D., Gentile G., Dettmar R.-J., Aronica G., Klein U., 2003, Astronomische Nachrichten Supplement, 324, 88

Xu C. K. et al., 2015, ApJ, 799, 11

This paper has been typeset from a TEX/LATEX file prepared by the author.